AD-A048 900 AIR FORCE INST OF TECH WRIGHT-PATTERSON AFB OHIO SCH--ETC F/G 20/4
OPTICAL INVESTIGATION OF FLOW FIELD GENERATED BY NORMAL SHOCK P--ETC(U)
DEC 77 S HUSSAIN

UNCLASSIFIED AFIT/GAE/AE/77D-5 NL

1 OF 1
ADA048900

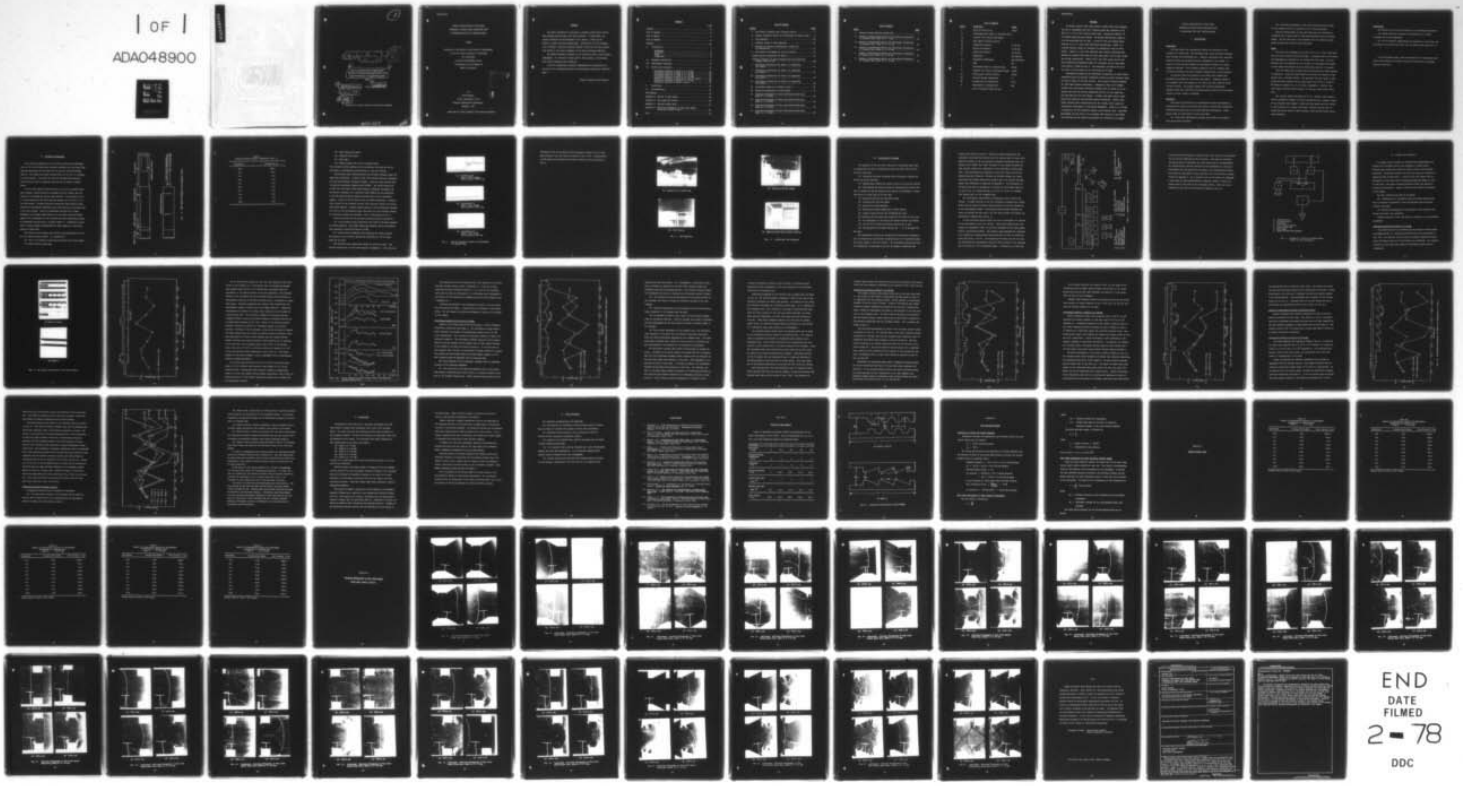

END
DATE FILMED
2-78
DDC

(1)

(9) Master's thesis,



(6)

# OPTICAL INVESTIGATION OF FLOW FIELD GENERATED BY NORMAL SHOCK PROPAGATING INTO A RECTANGULAR DUCT WITH IRREGULAR WALLS

THESIS

(10) Sajid Hussain
Flight Lieutenant P.A.F.

(14) AFIT/GAE/AE/77D-5

(11) Dec 77

(12) 80p.

Approved for public release; distribution unlimited

GAE/AE/77D-5

# OPTICAL INVESTIGATION OF FLOW FIELD GENERATED BY NORMAL SHOCK PROPAGATING INTO A RECTANGULAR DUCT WITH IRREGULAR WALLS

THESIS

Presented to the Faculty of the School of Engineering

of the Air Force Institute of Technology

Air University

in Partial Fulfillment of the

Requirements for the Degree of

Master of Science

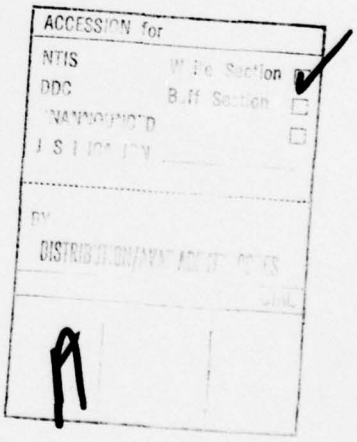


by

Sajid Hussain

Flight Lieutenant P.A.F.

Graduate Aeronautical Engineering

December 1977

Approved for public release; distribution unlimited

## Preface

The author expresses his gratitude to numerous people whose invaluable guidance and help made this study possible. In particular, the timely counseling and encouragement of Dr. Andrew J. Shine and Dr. Harold E. Wright are highly appreciated. Appreciation is also extended to Dr. William C. Elrod and Captain Richard A. Merz for the keen interest they showed in this work as members of the thesis advisory committee.

The useful assistance rendered by the laboratory staff is also highly commendable. Mr. William W. Baker and Mr. Leroy Cannon, in particular, were highly cooperative and receptive.

I wish to acknowledge my special indebtedness and appreciation to my wife for her unbounded patience and understanding during the "difficult days."

Flight Lieutenant Sajid Hussain

## Contents

## List of Figures

## List of Tables

## List of Symbols

| Symbol | Definition | Units |
|---|---|---|
| $a$ | Speed of Sound in Air | ft/sec |
| $M$ | Disturbance Mach Number in Irregular Duct | - |
| $M_i$ | Incident Test Section Mach Number | - |
| $M_s$ | Mach Number in Driven Section | - |
| $P_a$ | Atmospheric Pressure | in Hg abs. |
| $P_1$ | Driven Gas Pressure | in Hg abs. |
| $P_4$ | Driver Gas Pressure | in Hg abs. |
| $T$ | Temperature | deg Rankine |
| $T_a$ | Atmospheric Temperature | deg Fahrenheit |
| $t$ | Time | sec |
| $V$ | Disturbance Speed in Irregular Duct | ft/sec |
| $V_i$ | Incident Test Section Disturbance Speed | ft/sec |
| $V_s$ | Shock Speed in Driven Section | ft/sec |
| $\Delta X$ | Distance between Transducers | in |
| $\Delta t$ | Average Time to Traverse $\Delta X$ | $\mu$ sec |
| $\theta$ | Ramp Angle of Irregular Wall | deg |
| $\gamma$ | Ratio of Specific Heats for Air | - |

## Abstract

An optical study of flow field behind a normal shock wave propagating into a rectangular duct with irregular walls was conducted in the AFIT 8 in x 4 in x 20 ft air-air shock tube. Attenuation behavior of the normal shock was also studied. An average upstream Mach number of 1.59 was maintained for all runs. A total of five wall shapes designated as A, B, C, D and E were fabricated and analyzed. Model A, a straight section, served as reference for comparative study of other models. Models B, C and D had identical wave lengths, amplitudes and maximum and minimum flow areas but their ramp angle $\theta$ was 30 deg, 60 deg and 90 deg, respectively. Model E had a saw tooth design and all the other geometrical parameters except the wavelength and the ramp angle were similar to Models B thru D. The wavelength for Model E was half the value of other models and its ramp angle was 63 deg.

Disturbance attenuation was determined by measuring its speed across consecutive pairs of pressure transducers located at known distances along the entire length of the test section. Time interval counters measured the time lapse between transducers. Comparative study of all models revealed that disturbance attenuation depends upon the shape of the irregular wall and the two most significant factors in this regard are the ramp angle and the wave length. A higher ramp angle leads to more abrupt area reduction and provides greater attenuation. Shorter wave length provides more irregularities per unit length, which results in considerable improvement in attenuation phenomenon. Model D, $\theta$ = 90 deg is branded as the most effective design in the present study. Schlieren photographs of flow field in the irregular wall section for all models were obtained and the selected photographs are included in the report.

# OPTICAL INVESTIGATION OF FLOW FIELD GENERATED BY NORMAL SHOCK PROPAGATING INTO A RECTANGULAR DUCT WITH IRREGULAR WALLS

## I. Introduction

### Background

The term "shock wave attenuation" implies the reduction in the strength of a shock wave. This phenomenon has always attracted considerable interest from aerodynamicists. Numerous researchers have conducted detailed studies and suggested various techniques in this regard. A recent Air Force project required an experimental analysis of a newly suggested technique. This technique suggested that an irregular wall be used to attenuate the shock strength traveling down a closed channel.

The present study was proposed by the FCDNA Field Command Test Directorate, Kirtland Air Force Base, New Mexico. Different shapes of the irregular wall were required to be tested and their relative effectiveness studied. The present research was totally experimental. Whitham's Rule (Ref 12:337-360) provides methods by which the theoretical analysis of such a model is possible.

### Objective

This study was basically of an experimental nature and proposed to investigate the effects of various wall shapes on shock wave attenuation. Different wall models were to be fabricated and investigated. Fundamental modes of investigation in each case were:

(1) Shock speed measurements upstream and through the irregular wall across known distances

(2) Schlieren photographs of flow field along the entire length of the irregular wall at an interval of 20 to 30 microseconds.

Relative effectiveness of each wall shape was to be analyzed in comparison with a smooth wall of same cross-sectional area and overall length. All the tests were to be performed with the maximum incident shock strength that could be safely achieved.

## Scope

The tests were conducted in the AFIT 8 in x 4 in x 20 ft shock tube with air as the driver and the driven gas. A pressure ratio of 10 across the diaphragm was considered to be suitable for this study. Only one pressure ratio was employed so as to be able to investigate more number of wall shapes and because only high Mach number data was of interest.

Five wall shapes were studied, detailed description of which appears in Appendix A. Relative effectiveness of each wall was studied in comparison with a straight section. The amplitude and wave length of wall shapes were kept constant but the ramp angle $\theta$ was varied in steps of 30 degrees in models B, C, D, as shown in Appendix A. Model E, saw tooth shape, provided steady increase in flow area after abrupt reduction.

Test section length was limited to 19 in. However, these results could be extended to predict the shock attenuation over a greater length of the irregular wall channel. Shock tube Mach number was also limited to small values due to shock tube design. However, one may want to assume that shock waves of higher strength would display similar attenuation behavior.

Assumptions

The analysis of this study was based on the following assumptions:

(1) Normal shock wave entering the irregular duct is fully developed and is one dimensional

(2) For the range of temperatures and pressures in this study, the air behaves as a perfect gas with ratio of specific heats equal to 1.4.

In the succeeding pages, terms "disturbance" and "transmitted wave" refer to the balance of incident normal shock traveling in irregular portion of the duct.

## II. Equipment Description

The study was conducted in the Air Force Institute of Technology 8 in x 4 in x 20 ft shock tube, hereafter referred to as the shock tube. Detailed description of the shock tube is given by Davis and French (Ref 2). The driver and driven sections have an 8 in by 4 in rectangular cross section. The first four feet of the shock tube form the driver section which is separated from rest of the tube by a mylar sheet.

A 50 in test section fitted with two 6 in by 19 in optically flat glass windows, through which the irregular wall was visible, was connected to the extreme end of the driven section. The original 8 in by 4 in cross section of the shock tube was reduced to 4.5 in by 1 in in the test section. Pressure sensitive transducers Model PK14-15, manufactured by the Channel Industries, were flush mounted on the upper wall of the test section. First two transducers located 19.5 in apart determined the incident Mach number $M_i$ of the normal shock while Mach number of the disturbance in the irregular duct was determined by means of transducers located every 2 in apart (Table I). Transducers A and B (Fig. 1) were utilized for measuring the shock speed $V_s$ in the driven section of shock tube.

Flow field in the irregular wall section was photographed with the aid of a spark schlieren system. It consisted of:

(1) Two 9.5 in diameter concave mirrors having 30 in focal length

(2) High intensity spark lamp

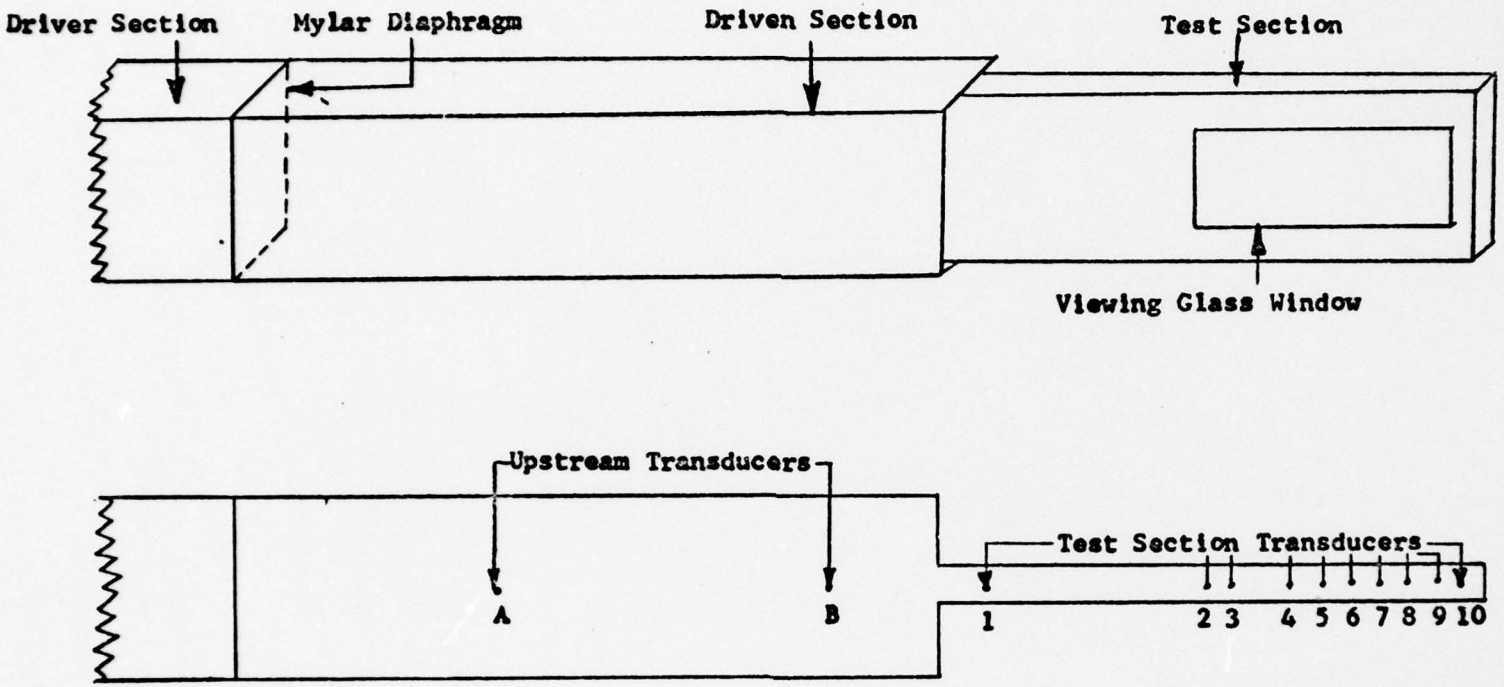


Fig. 1. Test Section Schematic and Transducer Layout

Table I
Distance Between Pressure Transducers (Fig. 1 )

| Transducers | Distance $\Delta X$ in. |
|---|---|
| A-B | 104.0 |
| 1-2 | 19.5 |
| 2-3 | 2.0 |
| 3-4 | 4.0 |
| 4-5 | 2.0 |
| 5-6 | 2.0 |
| 6-7 | 2.0 |
| 7-8 | 2.0 |
| 8-9 | 2.0 |
| 9-10 | 2.0 |

(3) Spark lamp power supply

(4) Optically flat mirror

(5) Knife edge

(6) Polaroid camera with type 47 polaroid film.

The schlieren optical system is on two platforms on wheels and can be positioned to photograph any desired part of the test section.

Oscilloscope model LA-265A provided the necessary delayed signal for spark lamp triggering. A total of four time interval counters registered the time lapse between transducer signals. Three of these counters were of Computer Measurement Company model CMC726C. The fourth counter was an Eput and Timer model 7360A manufactured by Beckman's Instrument Inc. Six Electro Instrument Inc. amplifiers model A20B-1 and two amplifiers of the SAD system provided necessary amplification of the transducer signals. A gain of 500 was used on all the A20B-1 amplifiers. Occasionally, results of the interval counters were verified by means of oscilloscope model LA-265A. Polaroid camera mounted on the oscilloscope recorded the trace on the oscilloscope screen from which the time interval between two transducer signals was inferred. This is illustrated in Fig. 2.

Driver and driven section pressure measuring system consisted of:

(1) A dial pressure gauge calibrated from 0-200 in Hg which measured the driver pressure. This gauge under-read slightly and the calibration curve revealed a correction factor of 0.997.

(2) U-tube mercury manometer which measured the driven pressure. The pressure value in driven section was maintained at -19.75 in Hg gauge for all runs.

Five different wall shapes were tested one after the other. The detailed description of these walls appears in Appendix A. Each wall was

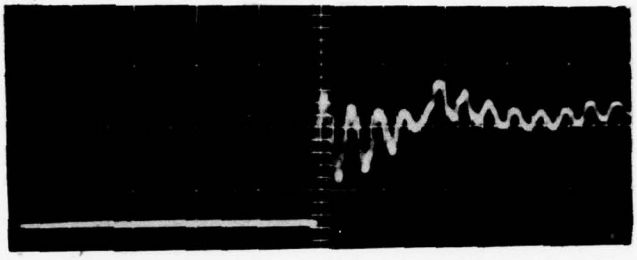

(a) Transducer A-B
Scale: 1000 μ sec/cm
Time Interval = 4800 μ sec

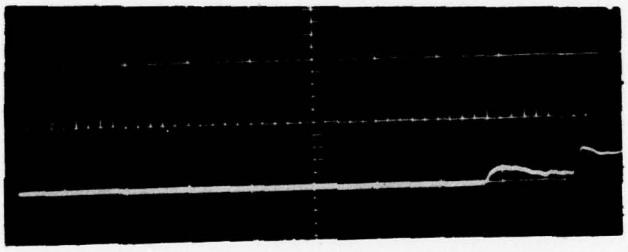

(b) Transducers 1-2
Scale: 100 μ sec/cm
Time Interval = 730 μ sec

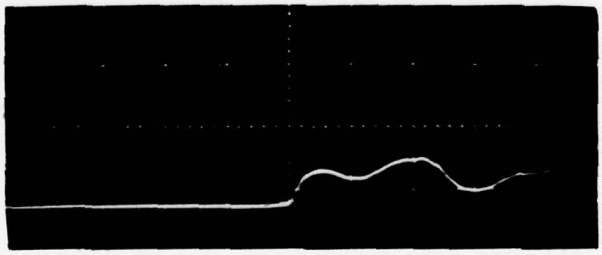

(c) Transducers 2-3
Scale: 10 μ sec/cm
Time Interval = 48 μ sec

Fig. 2 . Typical Transducer Traces on Oscilloscope for Elapsed Time

designed so that the irregular section appeared through the 19 in long glass window of the test section as shown in Fig. 3 (b). Irregularities in wall shape were repeated in the form of waves as can be observed in Fig. 6.

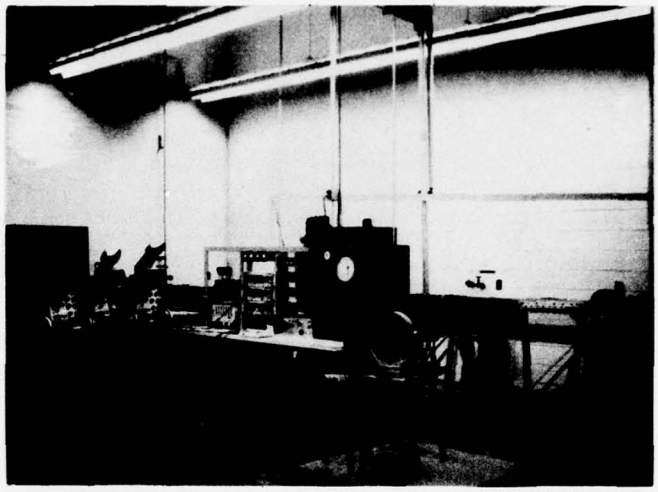

(a) General View of Shock Tube

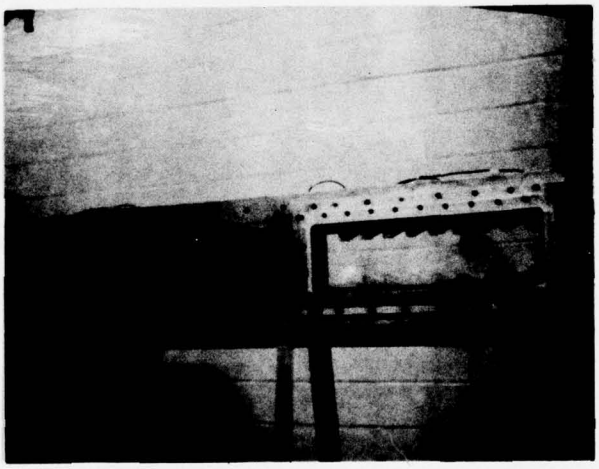

(b) Test Section

Fig. 3. Test Apparatus

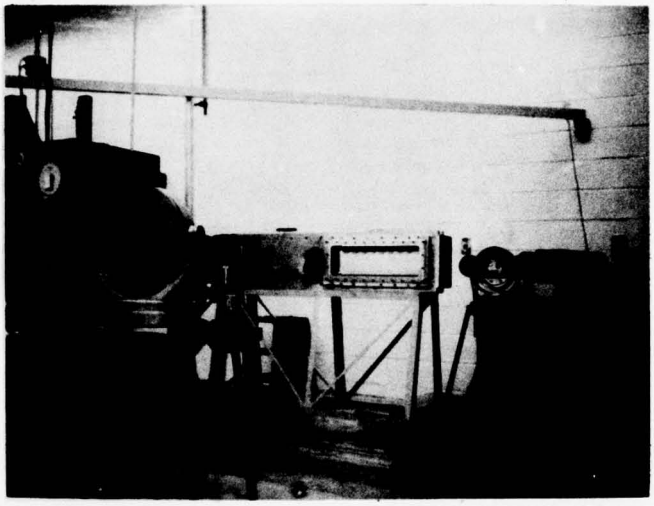

(c) Schlieren Optical System

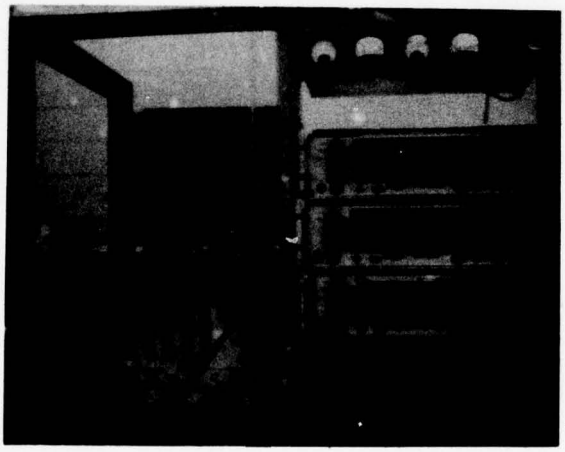

(d) Amplifiers and Time Interval Counters

Fig. 3 . (continued) Test Apparatus

## III. Experimental Procedure

The operation of the Air Force Institute of Technology shock tube is essentially the same as described by Davis and French (Ref 2:9-71). The basic steps are:

(1) Installing the mylar diaphragm after thoroughly cleaning the driver and driven sections

(2) Hydraulically locking the driven section to the driver section

(3) Pressurizing the driver section and evacuating the driven section to obtain the desired pressure ratio across the diaphragm. A pressure ratio of 10 was used in all the runs.

(4) Resetting counters and time delay units

(5) Switching off the room lights

(6) Opening the camera shutters

(7) Rupturing the mylar diaphragm by remote control

(8) Closing camera shutters and developing the film.

The following initial conditions existed at the start of each run:

(1) The temperature in the driver and driven sections was ambient

(2) The air in the driver and driven sections was at rest

(3) The pressure in the driven section was -19.75 in Hg gauge for all runs.

The fundamental criteria for assessing the disturbance attenuation was to determine its speed across consecutive pairs of transducers along the entire length of the test section. The disturbance speed across any two transducers was measured by the use of pressure transducers and

digital time interval counters. Electrical pulses generated by the transducers were amplified and fed into the counters and the delay units. Amplified signals of any two consecutive pressure transducers when connected to the 'START' and 'STOP' terminals of the counter provided the time interval between the transducers as the disturbance traveled past them. Each measurement was repeated at least four times and then the average time was determined. Knowing the distance between the transducers and the average elapsed time between them, the velocity and Mach number were calculated as explained in Appendix B. The transducers in the shock tube were so arranged as to furnish the disturbance speed $V_s$ in the 8 in by 4 in driven section, $V_i$ in the 4.5 in by 1 in reduced test section and V in the irregular duct.

The oscilloscope type LA-265A was frequently used to verify the results. A signal from one of the two transducers triggered the 'Single Sweep' and the second transducer pulse provided the vertical deflection on the oscilloscope screen. Oscilloscope mounted camera recorded the trace and knowing the time scale, the time lapse between two signals was determined as demonstrated in Fig. 2.

A spark schlieren optical system was used to photograph the location of the disturbance in the test section. Spark lamp triggering was controlled by transducer B (Fig. 1) which was connected to the signal delay device, oscilloscope LA-265A. The electric pulse generated by transducer B was delayed by a predetermined time period and fed into the schlieren spark lamp (Figs. 4 and 5). By readjusting the delay time for each run, the disturbance was photographed along the entire length of the irregular wall for every 20 to 30 microseconds delay. A reference 1 in long wire

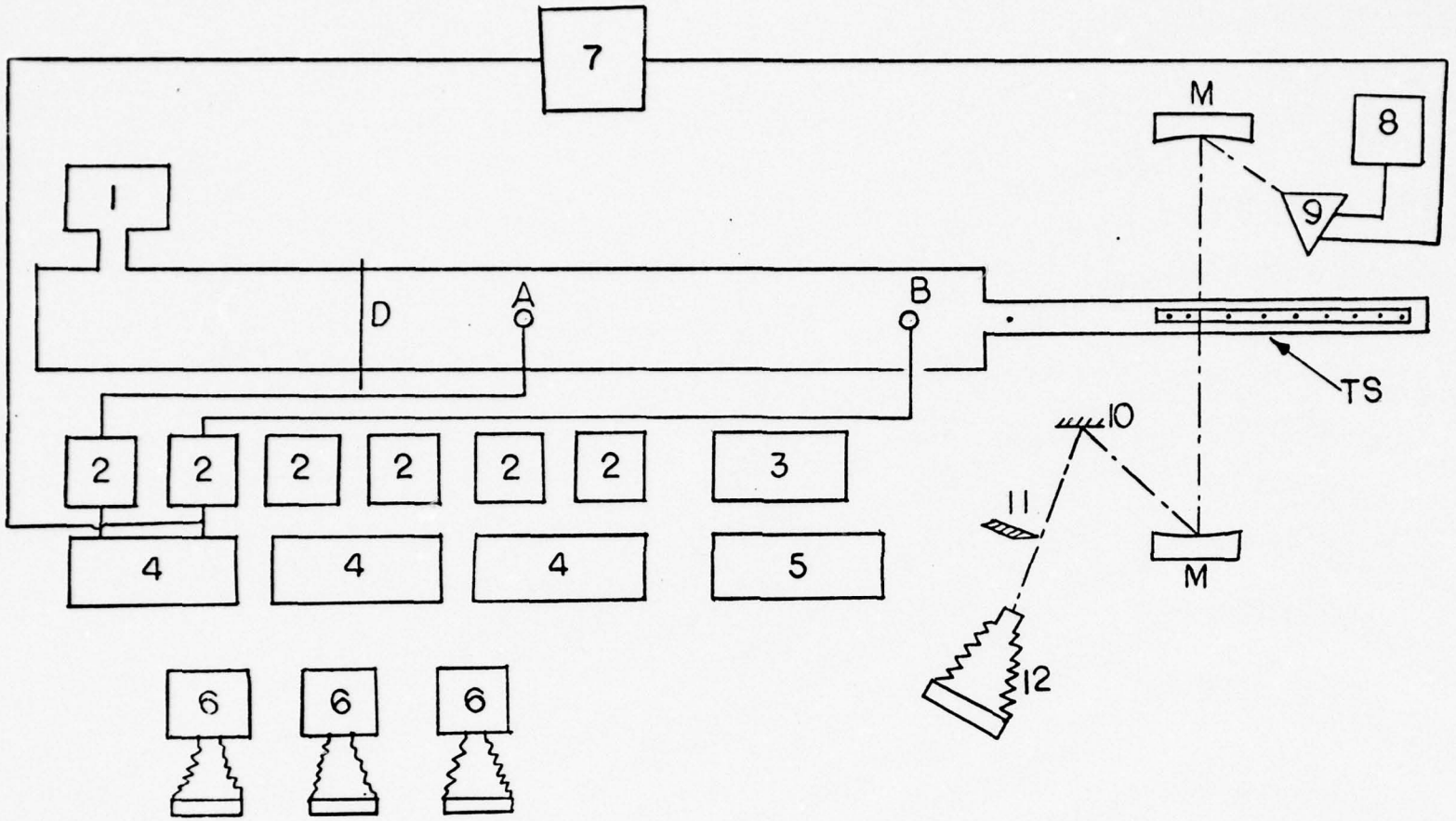


1. Air Supply
2. A20B-1 Amplifiers
3. SAD Amplifier
4. CMC 726C Counters
5. Beckman Counter
6. LA265A Oscilloscopes
7. Time Delay Unit LA-265A
8. Power Supply
9. Trigger Lamp
10. Plane Mirror
11. Knife Edge
12. Schlieren Camera

M. Schlieren Parabolic Mirrors
D. Diaphragm
A. thru B. Transducers
TS. Test Section

**Fig. 4 . Schematic Layout of Test Apparatus**

was used in each photograph to determine the scale factor which accounted for the picture magnification due to optics. Each time the schlieren system was moved or disturbed, the scale factor had to be redetermined. By correlating the relative location of the disturbance on a series of photographs with the respective time delays, the corresponding disturbance speed was determined at each location in the test section as demonstrated in Appendix B. For a pressure ratio of 10 across the diaphragm, a time delay of 1800 microseconds was typically needed to locate the normal shock at the start of the irregular section. This was true if transducer B was used as the reference transducer (Fig. 4).

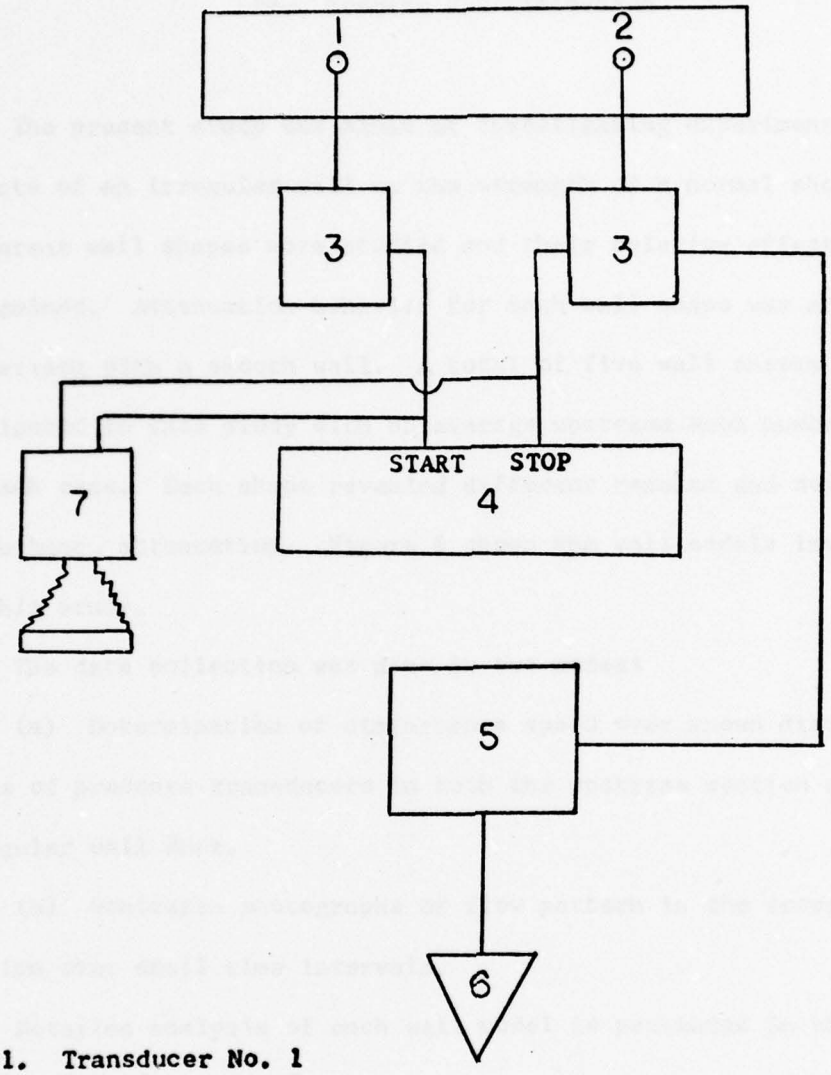


1. Transducer No. 1
2. Transducer No. 2
3. Amplifiers
4. Time Interval Counter
5. Signal Delay Unit
6. Spark Lamp
7. Camera Mounted Oscilloscope

Fig. 5. Schematic of Typical Instrumentation Layout for Two Transducers

## IV. Results and Discussion

The present study was aimed at investigating experimentally the effects of an irregular wall on the strength of a normal shock. Different wall shapes were studied and their relative effectiveness determined. Attenuation behavior for each wall shape was analyzed in comparison with a smooth wall. A total of five wall shapes were investigated in this study with an average upstream Mach number of 1.59 in each case. Each shape revealed different results and degrees of disturbance attenuation. Figure 6 shows the wall models investigated in this study.

The data collection was done in two modes:

(a) Determination of disturbance speed over known distances by means of pressure transducers in both the upstream section and the irregular wall duct.

(b) Schlieren photographs of flow pattern in the irregular wall section over small time intervals.

Detailed analysis of each wall model is presented in the succeeding paragraphs.

### Disturbance Analysis in Model A, $\theta$ = 0 Deg

This model was used as a reference and the results of other models were compared with it. Attenuation behavior for this case appears in Fig. 7(a). The abscissa shows the pair of pressure transducers across which the average speed of the disturbance was determined. The ordinate consists of the average Mach number of disturbance across pairs of transducers.

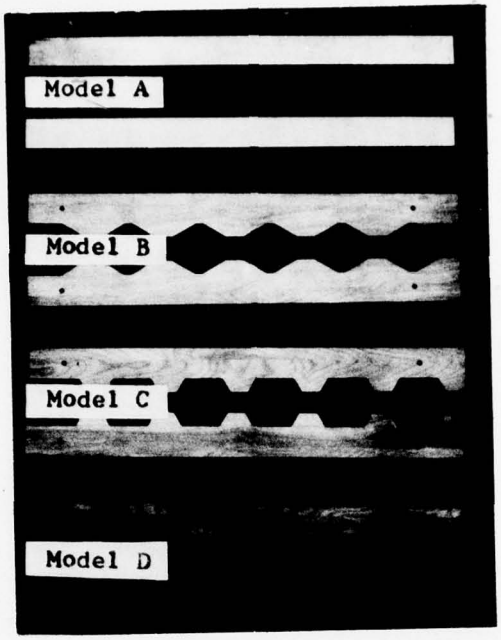


(a) Models A thru D

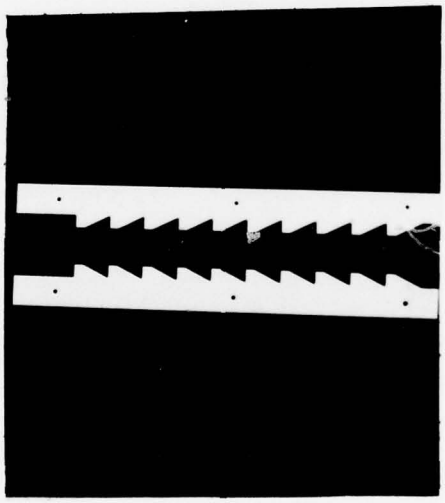

(b) Model E

Fig. 6. Wall Shapes Investigated in the Test Section

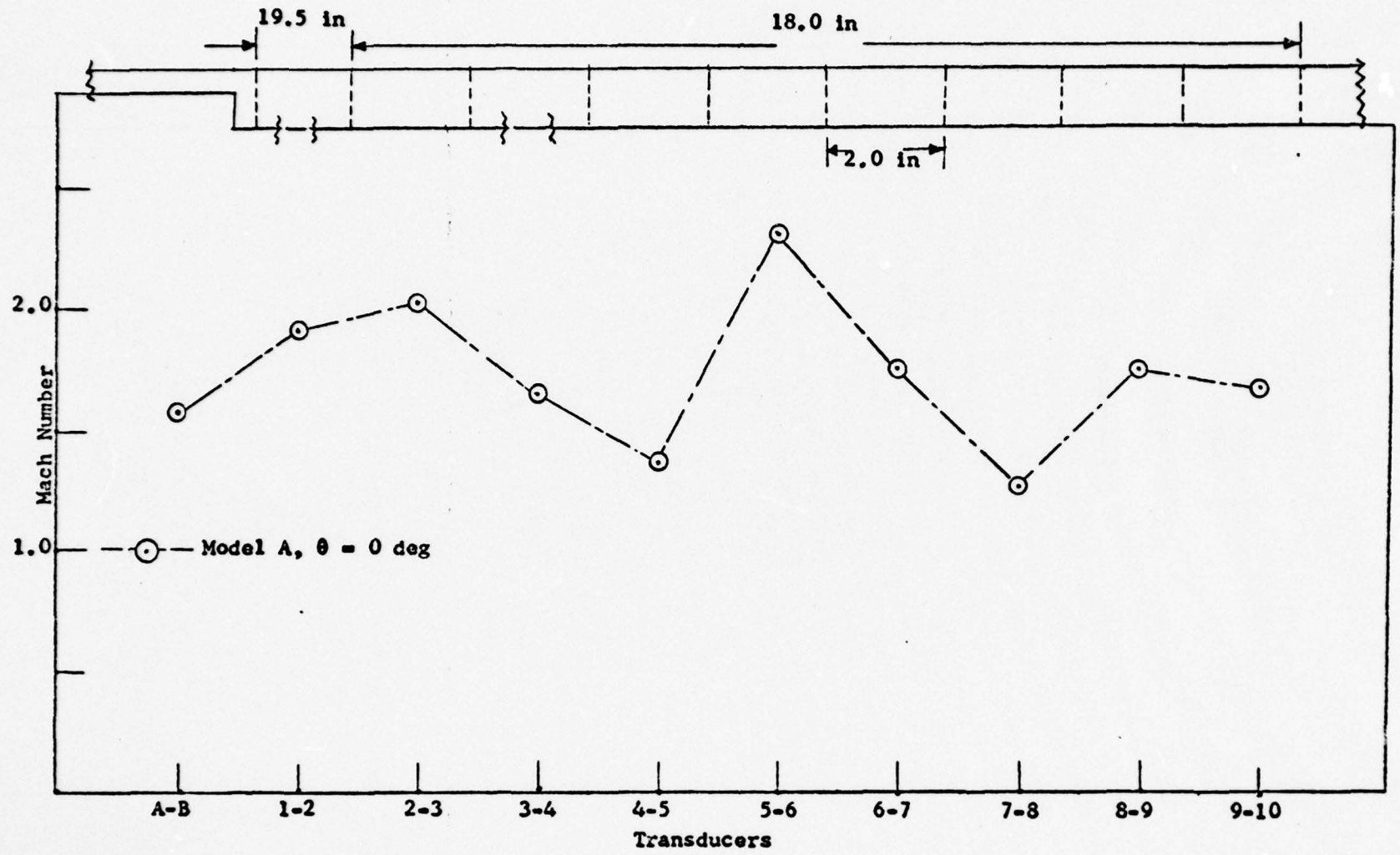


Fig. 7(a). Disturbance Attenuation for Model A

For an incident Mach number of 1.92, Fig. 7(a) depicts a cyclic behavior in the strength of the disturbance with the maximum and minimum Mach numbers being 2.32 and 1.27, respectively, indicating that the disturbance in the reduced section is not yet stabilized. This unstable behavior is in contradiction with the Whitham Theory, which predicts an instantaneous increase in the shock strength after it encounters an abrupt area change. Whitham's assumption has, however, been disproved by the experimental results of Peters (Ref 7) and Tambra (Ref 11). Tambra had investigated the effects of an abrupt area reduction on the strength of a moving shock wave. He had studied a number of area ratios and the consequent effect of each on the shock strength, as obtained from Ref 11, is graphically presented in Fig. 7(b). Peters in his study had experimentally analyzed the effects of a convergent channel on the shock strength. According to their research, in particular the study of Tambra, the shock strength does not attain the maximum increase immediately after area reduction but it does so some distance down the reduced section. Tambra's research also clearly reveals a cyclic behavior in the strength of the shock wave in the reduced section (Fig. 7(b)). In the present study, flow area of 32 $in^2$ in the driven section was reduced to 4.5 $in^2$ in the test section between transducers 1 and 2 (Fig. 1). Oscillatory behavior of the shock strength is thus in agreement with the experimental results of Tambra and Peters.

For an area reduction from 32 $in^2$ to 4.5 $in^2$ and the initial Mach number of 1.58, Whitham's Rule predicts a Mach number of 1.71 in the reduced section. Experimental data, however, reveals an average Mach number of 1.92 in the reduced section between transducers 1 and 2 (Fig. 1), showing an error of 11.8% between theoretical predictions of Whitham and the experimental results.

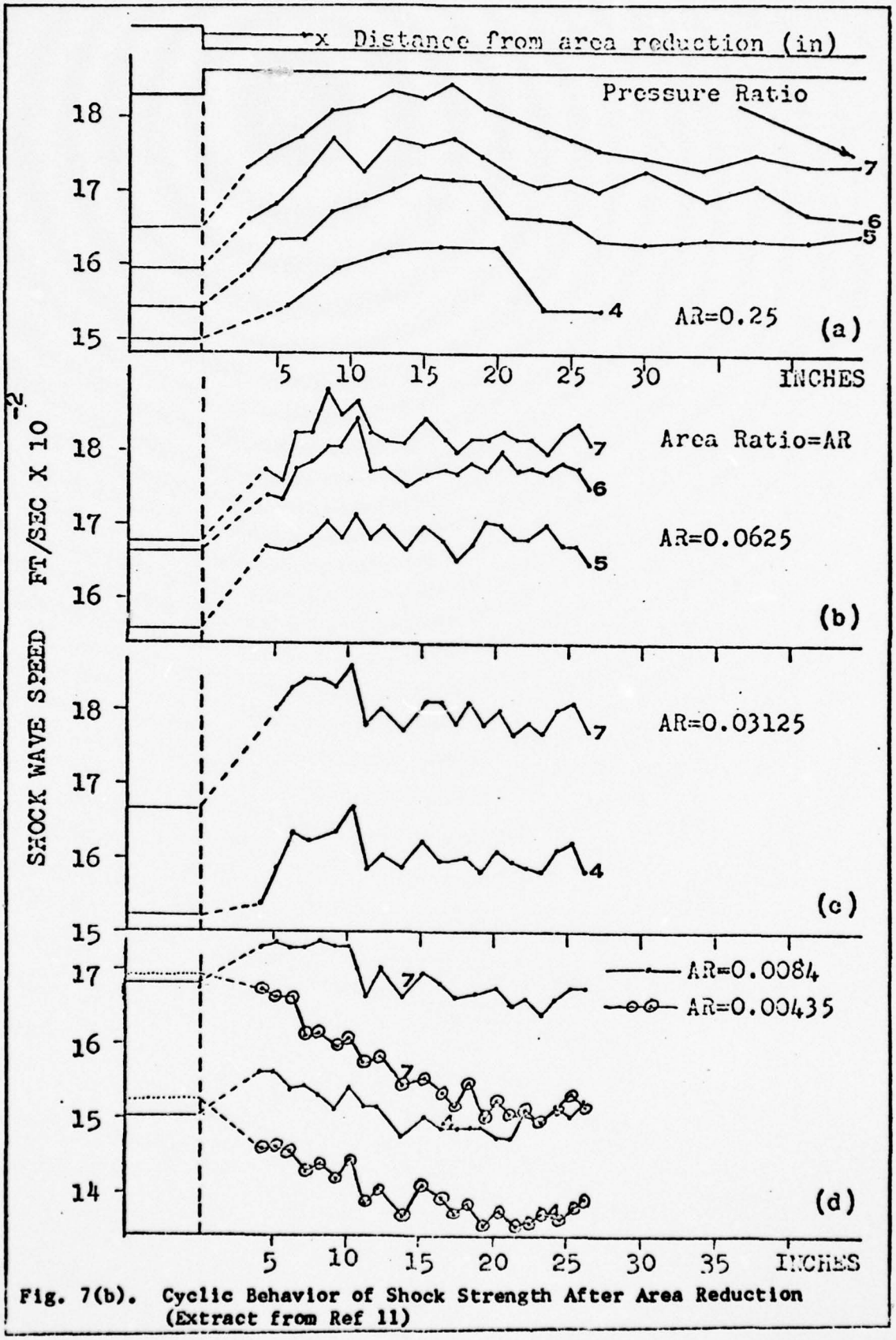


**Fig. 7(b). Cyclic Behavior of Shock Strength After Area Reduction (Extract from Ref 11)**

The maximum flow area for Models B thru E was identical to the flow area for straight channel, Model A (Appendix A). Since the initial conditions up until transducer number 2, i.e., start of the irregular wall, were the same for all models, it is considered quite reasonable to use Model A as the reference for comparative study of wall shapes B thru E (Appendix A).

Schlieren photographs of the disturbance in Model A did not reveal any interesting wave forms. A normal shock was displayed in each photograph. For this reason no schlieren photographs of Model A are included in this report.

Disturbance Analysis in Model B, $\theta$ = 30 Deg

Model B, with a ramp angle of 30 deg, displays a totally different disturbance attenuation than Model A. The disturbance strength shows a cyclic behavior with maximum and minimum Mach numbers being 2.75 and 0.63, respectively. Fig. 8 gives the comparative behavior of Model B in relation to Model A. The disturbance strength variation is more severe than the straight channel and the minimum value of Mach number obtained in this model is far below the value for Model A. In the last part of the irregular wall, however, the disturbance strength displays an increasing tendency and the maximum value of the Mach number reaches to 2.75. This increase cannot be explained with the existing data.

The cyclic behavior of the disturbance strength could be explained by means of the following arguments:

(1) The interaction of the moving disturbance with an area reduction produces transverse waves which travel in a direction normal to the path of the incident normal shock. These transverse waves travel to the

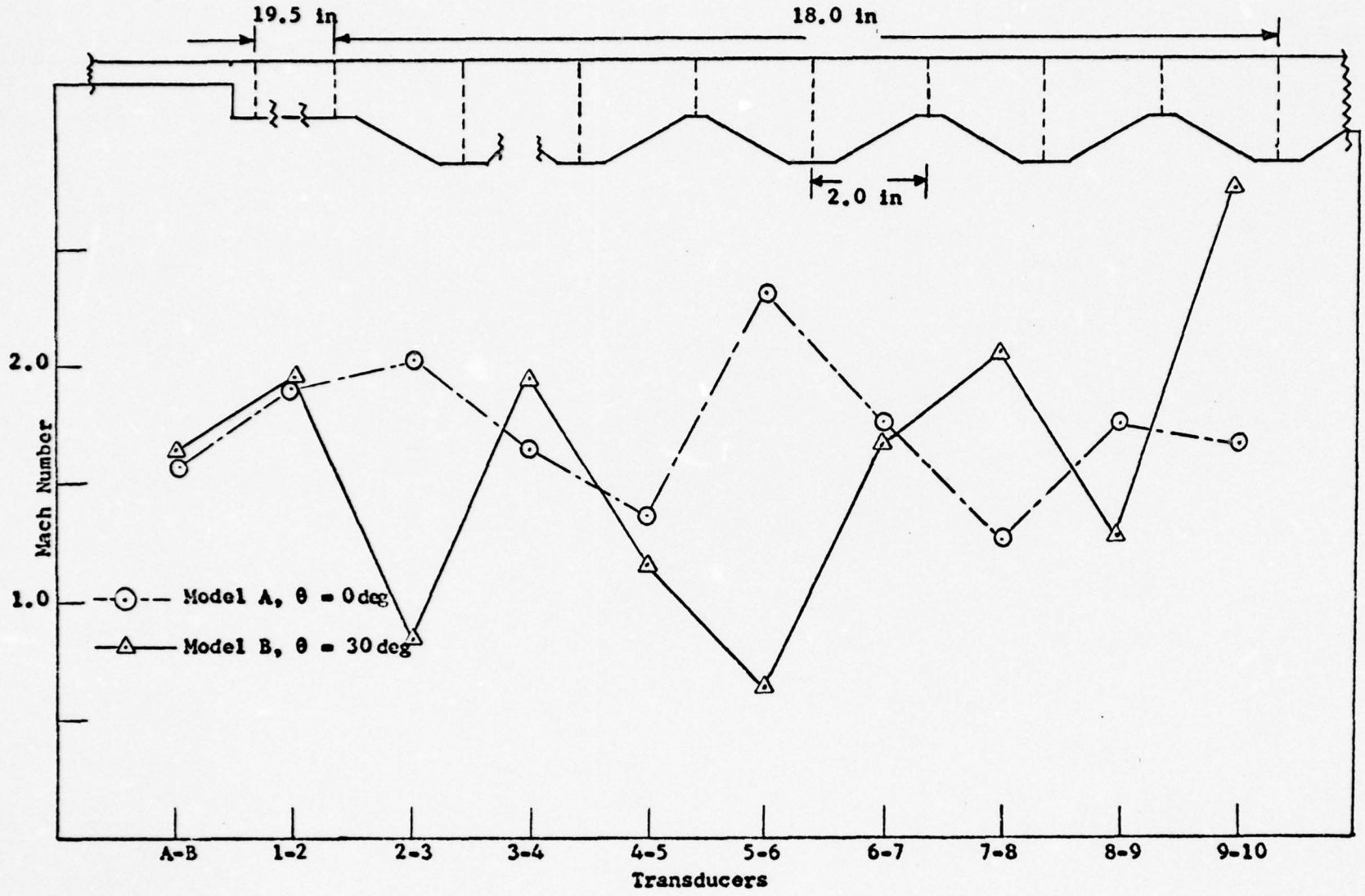


Fig. 8. Disturbance Attenuation for Model B in Comparison with Model A

opposite wall and then reflect. As a consequence, an additional increment of pressure is imparted to the flow field enclosed between the transverse wave and the transmitted wave. This pressure increase behind the transmitted wave tends to increase the disturbance strength locally.

(2) The increase in flow area provided by the divergent portion of the irregular wall tends to reduce the effective strength of the disturbance.

(3) Physical obstruction to the disturbance and the wall friction, induce reduction in its strength near the wall.

(4) As observed in Model A (Fig. 7(a)), the disturbance strength shows an oscillatory behavior. Thus the incident wave itself is unstable and when superimposed on the above condition leads to discrete jumps in its strength.

(5) Due to small wavelength of the irregular wall, the transverse waves explained in (1) above fail to stabilize since more transverse waves are being continuously generated by the irregular wall. The transverse waves attenuate over a period of time but their oscillations produce oscillations in the strength of the transmitted disturbance.

The disturbance strength shows another interesting and unusual behavior. According to the known theories of Whitham (Ref 12) and Shapiro (Ref 10), the disturbance strength should increase with the reduction in flow area and reduce with increase in flow area. This phenomenon is not depicted entirely in this study. In certain instances, the disturbance strength has decreased with decrease in flow area. For instance, the value of the Mach number between transducers 5-6 (convergent portion) is less than the value between transducer 4-5 (divergent portion) as shown in Fig. 8. This, however, cannot be regarded as a violation of the

theories of Whitham and Shapiro since the chain of transverse waves generated by each irregularity on the wall contradicts the conditions under which the theories hold.

Schlieren photographs of flow field in the irregular wall are shown in Fig. 14. For each photograph, transducer B (Fig. 4) was used as the reference transducer for delay time settings. As observed in Fig. 14(a), the incident disturbance is a perfectly normal shock. As it impinges on the irregular wall: (a) a portion of the shock is reflected back from upper and lower surfaces of the wall and travels upstream, (b) transverse waves are generated, one each, from upper and lower surfaces of the wall. These waves propagate normal to the direction of incident normal shock, (c) balance of normal shock travels down the test section as a transmitted wave, also referred to as disturbance.

The transverse waves travel toward the opposite walls and in doing so add incremental pressure behind the transmitted wave. This addition tends to accelerate the portion of transmitted wave affected by the transverse wave. Figure 14(b) indicates how the transmitted wave near the wall is bent forward due to the local increase in its strength. After the transverse waves have traveled the entire height of the flow area, the shape of the entire transmitted wave changes. Subsequent pictures of Fig. 14 reveal that the transmitted wave is curved and portions of the wave adjacent to the wall tend to follow behind. This comes about due to the physical obstruction to flow and the wall frictional effects.

Each irregularity on the wall generates a pair of transverse waves which attenuate with time and cluster together to form more and more complicated wave forms, as can be seen in Fig. 14(j). The formation of

boundary layer behind the transmitted wave and its interaction with normal shocks and the subsequent turbulence can be observed in Fig. 14(i) and (p).

Disturbance Analysis in Model C, $\theta$ = 60 Deg

This model provided a more abrupt reduction in flow area than Model B. The effects of this model on disturbance strength appear in Fig. 9 in comparison with the straight channel. Cyclic behavior in disturbance strength is obvious from the figure. Values of disturbance Mach number fluctuate between a maximum and minimum of 2.31 and 0.74, respectively. Model C showed an improvement over Model B, particularly in the last portion of the irregular wall. The flow field as analyzed by the pressure data and optical system is more complex and as such would be expected to show greater attenuation than the straight channel. This is weakly confirmed in Fig. 9.

The flow field photographed by means of the schlieren optical system is depicted in Fig. 15. The incident wave is once again perfectly normal. Interaction of incident wave with the irregular wall generates a pair of transverse waves which travel normal to the flow direction. The historical progression of typical transverse waves can be observed in Fig. 15(a) through (d). Due to the pressure increase behind the transmitted wave, induced by the transverse waves, portions of the transmitted wave tend to accelerate and as a result bend forward as observed in Fig. 15 (b), (c) and (d).

Ordinarily the transverse waves impart incremental pressure behind the entire transmitted wave until the transverse waves attenuate sufficiently. In the present design, however, successive transverse waves are being generated by each irregularity on the wall leading to an extremely complex system of transverse waves trailing behind the transmitted wave as observed in Fig. 15 (l), (m) and (r).

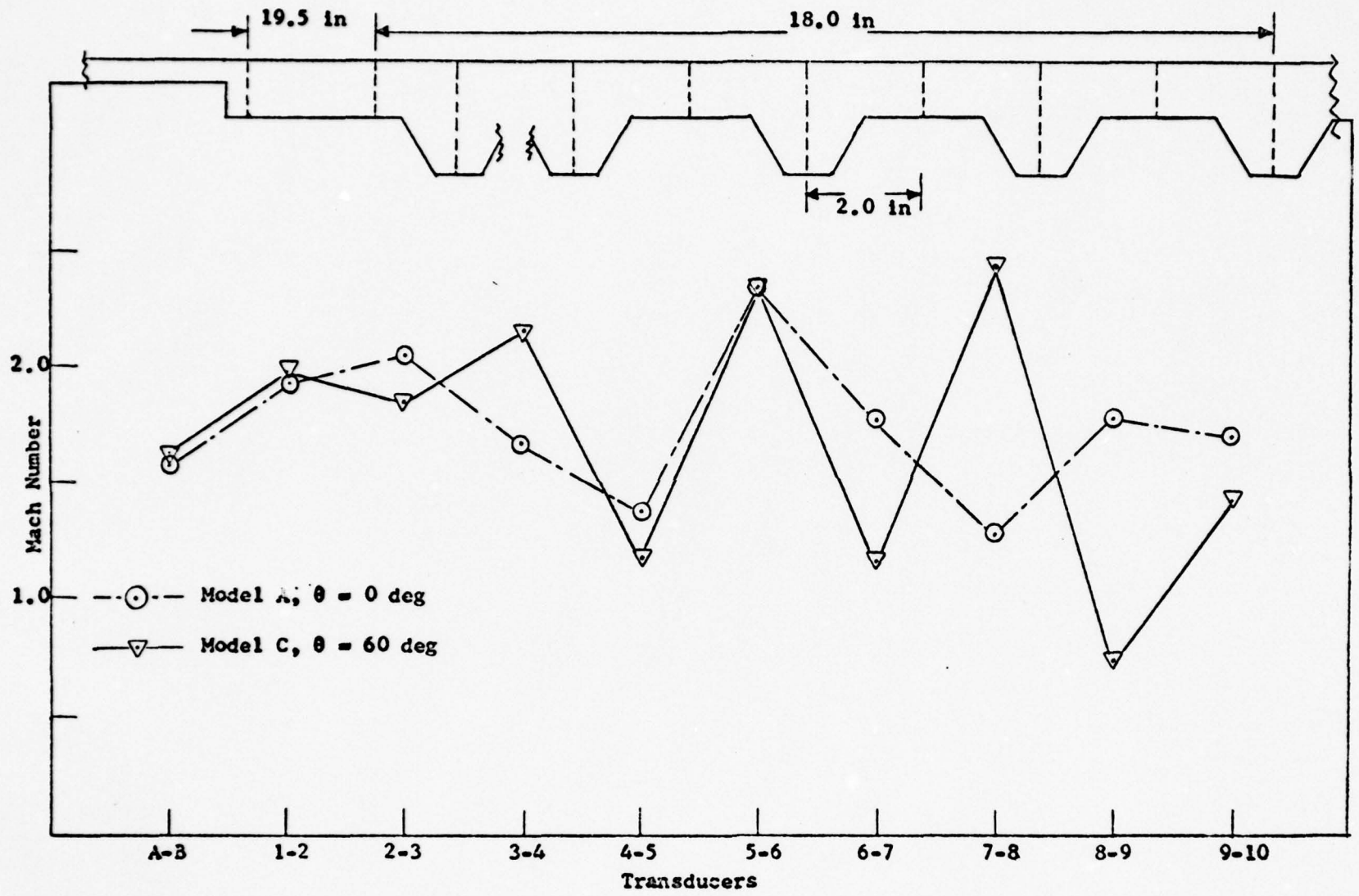


Fig. 9. Disturbance Attenuation for Model C in Comparison with Model A

As is obvious from part (e) onwards of Fig. 15, the shape of the transmitted wave no longer remains normal, and portions of the transmitted wave near the wall bend backwards and travel at a lower speed than the rest of the disturbance.

Boundary layer formation behind the transmitted wave and the turbulence therein is clearly observed in Fig. 15 (k), (m), (p) and (t) over flat and inclined surfaces of the wall.

Disturbance Analysis in Model D, $\theta = 90$ Deg

Model D offered an abrupt area reduction from 4.5 $in^2$ to 3.0 $in^2$ followed by an abrupt increase in flow area from 3.0 $in^2$ to 4.5 $in^2$ (Appendix A). Attenuation behavior for this model is shown in Fig. 10. The cyclic attenuation behavior observed in case of Models A, B and C is replaced by a relatively smooth and consistent downward trend. Disturbance Mach numbers vary between the maximum and minimum values of 2.32 and 0.42, respectively. Figure 10 displays a great reduction in disturbance strength in comparison with Model A. In addition, the disturbance strength shows a continuous decline along the test section until the Mach number essentially stays constant beyond transducer number 7.

Schlieren photographs of flow field for Model D appear in Fig. 16. The incident normal shock interacts with abrupt area reduction generating two transverse waves which travel normal to the flow direction towards opposite walls (Fig. 16 (a) thru (d)). The length of normal shock wave reduces as the transverse waves sweep across the flow area until ultimately the entire transmitted wave becomes curved. Further interaction of the transmitted wave with the irregular wall generates a series of transverse waves which produce an extremely complicated wave form behind

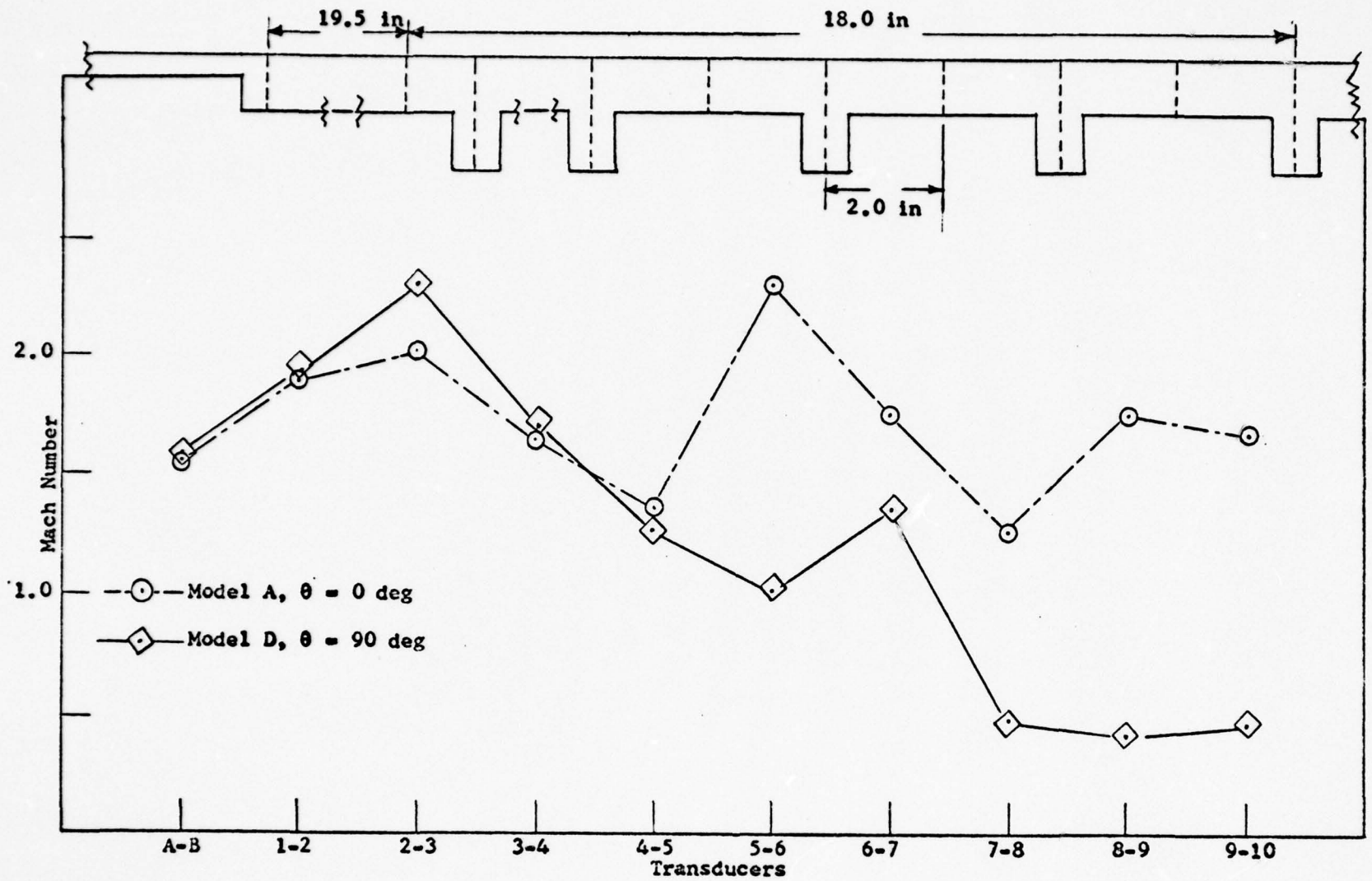


Fig. 10. Disturbance Attenuation for Model D in Comparison with Model A

the transmitted wave as observed in Fig. 16(r). The abrupt area reduction and wall frictional effects tend to decelerate the portion of transmitted wave in the vicinity of irregular wall and that portion appears to be trailing behind. This phenomenon can be observed in all pictures beyond (e) in Fig. 16. Turbulent areas in the flow behind the transmitted wave are prominently visible in Fig. 16(n), (o) and (s).

Summary of Disturbance Analysis for Models B thru D

Figure 12 displays the relative attenuation for all of the five models investigated in this study. For Models B, C and D, wavelength, amplitude and maximum and minimum flow areas were the same (Appendix A). The only variable parameter in these models was the ramp angle $\theta$. Comparative study of Fig. 12 reveals that a higher ramp angle $\theta$ results in a greater disturbance attenuation.

Disturbance Analysis in Model E, $\theta = 63$ Deg

This model combined the features of Models B thru D. It provided an abrupt area reduction from 4.5 $in^2$ to 3 $in^2$ followed by a steady increase in the flow area to 4.5 $in^2$ (Appendix A). The wavelength was, however, smaller than other models and consequently there were more number of irregularities in the wall.

Figure 11 describes the relative attenuation of this model in comparison with the straight section. Mach number variations are between the maximum and minimum values of 2.0 and 0.1, respectively. As is apparent from this figure, Model E reduces the disturbance strength much more effectively than Model A. It is also obvious from the figure that Mach numbers observed in this model are extremely low, in fact

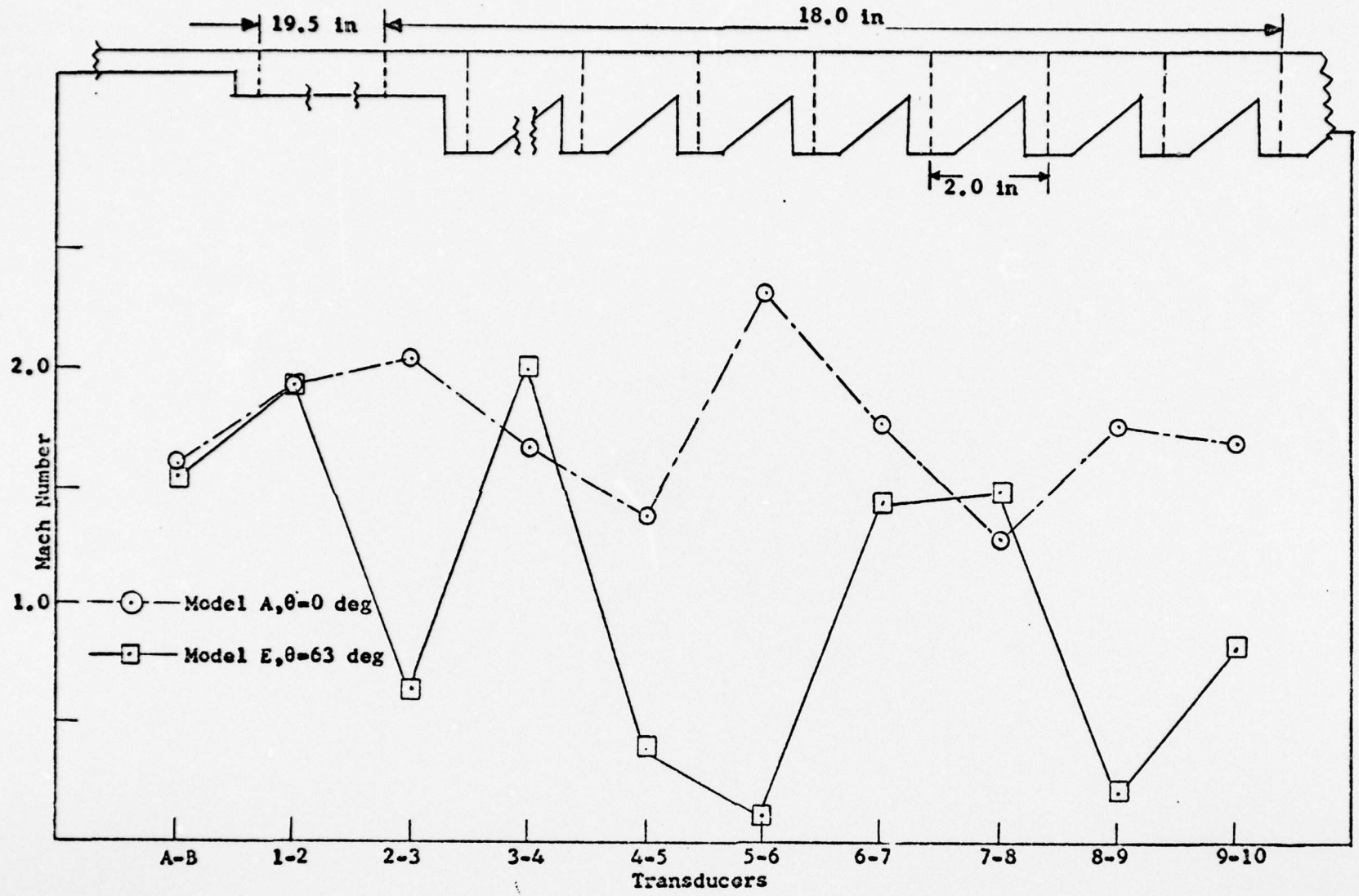


Fig. 11. Disturbance Attenuation for Model E in Comparison with Model A

lower than any of the previous models investigated in this study (Fig. 12). This could be attributed to the fact that in Model E there were more number of repeated irregularities than other models.

Pictorial history of wave forms in the irregular section is shown in Fig. 17. Once again the normal incident shock upon encountering the abrupt area reduction leads to the following sequence of events: (1) portion of the shock wave is reflected upstream due to the obstruction at upper and lower surfaces of the wall, (2) transverse waves are generated and they propagate normal to the flow direction, (3) the balance of the incident shock continues to travel downstream as transmitted wave. Each subsequent irregularity generates a pair of transverse waves which alternately reflect from the upper and lower surfaces of the irregular wall and generate extremely complex flow field behind the transmitted wave as can be observed in Fig. 17(d), (g) and (j). Beyond part (a) of Fig. 17 the transmitted wave is curved and the portions of this wave near the upper and lower surfaces of the irregular section appear to travel at a lower speed. Turbulent regions of flow field behind the transmitted wave can be observed in Fig. 17(f), (j), (k) and (m). Flow region behind the transmitted wave after sufficient time lapse looks like Fig. 17(n), (o) and (p).

Comparative Analysis of Models A thru E

A comparative study of Fig. 12 reveals the following:

(a) The disturbance strength in the straight section (Model A) shows a cyclic behavior which is in agreement with the experimental results of Tambra (Ref 11) and Peters (Ref 7).

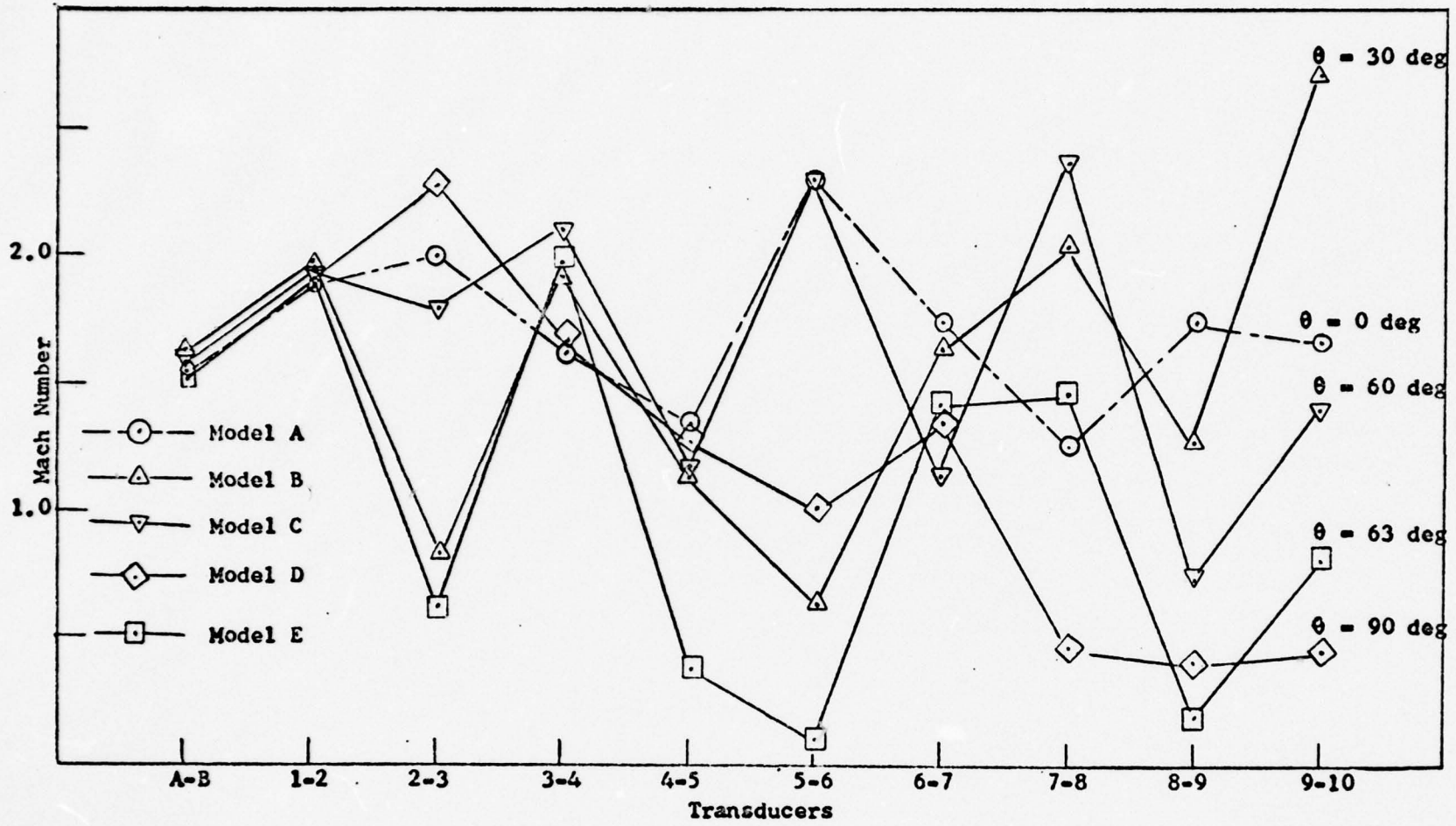


Fig. 12 . Disturbance Behavior for Models A thru E

(b) Model B with a ramp angle θ of 30 deg shows a significant attenuation trend in the initial part of the irregular section. It, however, indicates an undesirable increase in the disturbance strength in the last part of irregular duct.

(c) Model C depicts a better attenuation trend than Models B and A. The Mach number fluctuations are, however, more severe in this model.

(d) Model D shows a definite improvement over the above three models. The disturbance strength reduces continuously down the test section until it assumes an essentially constant value beyond transducer number 7.

(e) Model E shows a positive edge over Models A thru C. It achieves Mach number values far below the ones obtained in any of the other four models.

In order to recommend the most effective model for disturbance attenuation the following criteria will be adhered to: "The wall shape which provides smooth and consistent trend in shock attenuation and weakens the disturbance in the minimum possible distance, would be considered to be the most effective."

On the basis of this criteria Model D, $\theta = 90$ deg is recommended for achieving best results in disturbance attenuation. It could, however, be assumed that the results for Model D may be further improved by reducing the wavelength in the irregular wall from 4 in to 2 in (Appendix A) while keeping the rest of the parameters the same.

The results for pressure data demonstrated good repeatability. The data scatter in most runs was less than 4% while a few cases showed scatter as great as 10%. Pressure data was obtained primarily by means of electronic time interval counters. Disturbance speed measurements from the schlieren photographs (Appendix A) were used only for the purpose of verification of data obtained from time interval counters. Schlieren photographs cannot be recommended as an accurate means of disturbance speed measurement.

## V. Conclusions

The purpose of this study was to optically investigate the flow field behind a normal shock propagating into a duct with irregular walls. The shock speed was also determined across known distances in the irregular channel. The Air Force Institute of Technology shock tube was employed in this study. Five different wall shapes (Appendix A) were investigated in the order given below:

(a) Model A, $\theta = 0$ deg
(b) Model B, $\theta = 30$ deg
(c) Model C, $\theta = 60$ deg
(d) Model D, $\theta = 90$ deg
(e) Model E, $\theta = 63$ deg.

In each of the above cases the initial conditions upstream of the test section were identical.

Relative study of the above models in comparison with the straight section revealed that the disturbance strength attenuates in an irregular wall and the degree of attenuation depends on the shape of the wall. Dependence of disturbance attenuation upon the ramp angle $\theta$ was also distinctly observed. Walls with higher ramp angles displayed a greater attenuation behavior.

The results of Model A indicated a cyclic behavior in disturbance strength although such a behavior is not predicted by Whitham's Theory (Ref 12). This behavior is, however, consistent with the experimental results of Tambra (Ref 11) and Peters (Ref 7). Comparison of results obtained for Models B thru D displayed one important feature: strength of the disturbance depends directly upon the abruptness of area change in

the flow region. Model D offered greater attenuation than Model C which in turn showed an improvement over Model B.

Model B depicted a hopeful attenuation trend in the beginning of the irregular duct but in the later part it demonstrated a substantial increase in disturbance strength. No conclusive opinion can be expressed about this behavior due to limited length of the test section. It is, however, expected that tests conducted on this model over longer lengths of irregular wall would lead to more definite results.

In Models B, C and D the wavelength, amplitude and maximum and minimum flow areas were the same but the ramp angle $\theta$ was different. Model E combined the features of all the other models.

Relative study of all models indicated that Models D and E were extremely effective in attenuating the disturbance strength (Fig. 12). Model D, however, had a slight edge over Model E since it displayed a smooth, consistent and rapid decline in the disturbance strength. Mach number fluctuations were minimum for Model D.

For the purposes of this study, Model D has been chosen as the most effective design for disturbance attenuation. It is, however, suggested that the wavelength in this model be reduced from 4 in to 2 in, the results of which are expected to reveal much better results.

## VI. Recommendations

The following recommendations are submitted:

(1) The tests may be conducted at other pressure ratios to determine the effect of incident Mach number on shock wave attenuation.

(2) Amplitude and wavelength of the existing model could be altered and the consequent attenuation studied.

(3) Length of the irregular duct could be increased and its effectiveness analyzed practically.

(4) It is expected that a porous irregular duct would considerably enhance the shock wave attenuation. It is therefore suggested that further tests be conducted with this arrangement.

(5) Further tests may be conducted with existing models by mounting the pressure transducers on the flat wall of the irregular duct.

## Bibliography


1. Bernstein, L. "Some Measurements of Shock-Wave Attenuation in Channels of Various Cross-Sections." Aeronautical Research Council, ARC 22,619 Hyp. H3 (1961).

2. Davis and French. Design and Construction of a Shock Tube. Thesis. Wright-Patterson Air Force Base Ohio: Air Force Institute of Technology, August 1955.

3. Eheart, R. L. Attenuation of Weak Shock Waves in a Non-Uniform Region. Thesis. Wright-Patterson Air Force Base, Ohio: Air Force Institute of Technology, March 1973.

4. Glass, I. I. "Theory and Performance of Simple Shock Tubes." UTIA Review, No. 12, Part I, Institute of Aerophysics, University of Toronto, Canada (May 1958).

5. Hall, J. G. "Production of Strong Shock Waves; Shock Tube Applications, Design, and Instrumentation." UTIA Review, No. 12, Part II, Institute of Aerophysics, University of Toronto, Canada (May 1958).

6. Heinrich, R. D. Experimental Shock Tube Study of Attenuation of Weak Shock Wave. Thesis. Wright-Patterson Air Force Base, Ohio: Air Force Institute of Technology, December 1972.

7. Peters, M. H. The Interaction of Moving Shock with the Convergent Section in a Shock Tube. Thesis. Wright-Patterson Air Force Base, Ohio: Air Force Institute of Technology, March 1969.

8. Rhode, R. H. Effect of Inlet Contour on the Interaction of a Shock with a Reduced Section in a Shock Tube. Thesis. Wright-Patterson Air Force Base, Ohio: Air Force Institute of Technology, March 1971.

9. Rosciszewski, J. J. "Calculation of the Motion of Non-Uniform Shock Waves." Journal of Fluid Mechanics, 11: 337 (1961).

10. Shapiro, A. H. The Dynamics and Thermodynamics of Compressible Fluid Flow. Volume I and II. New York: The Ronald Press Company, 1954.

11. Tambra, M. L. The Interaction of Moving Shock with an Abrupt Area Reduction in a Shock Tube. Thesis. Wright-Patterson Air Force Base, Ohio: Air Force Institute of Technology, March 1970.

12. Whitham, G. B. "On the Propagation of Shock Waves Through Regions of Non-Uniform Area of Flow." Journal of Fluid Mechanics, 4: 337 (1958).

## Appendix A

### Details of Wall Shapes

Figure 13 describes the general shapes and nomenclature of the walls investigated in this study. They are categorized as A, B, C, D and E and their numerical details are tabulated below:

| Wall Shape | A | B | C | D | E |
|---|---|---|---|---|---|
| Ramp Angle $\theta$ deg | 0 | 30 | 60 | 90 | 63 |
| Distance Between Transducers $\Delta x$ in | 2 | 2 | 2 | 2 | 2 |
| Wavelength $\ell$ in | - | 4 | 4 | 4 | 4 |
| Maximum Amplitude h in | - | 0.75 | 0.75 | 0.75 | 0.75 |
| Minimum Flow Area $A_{min}$ $in^2$ | - | 3 | 3 | 3 | 3 |
| Maximum Flow Area $A_{max}$ $in^2$ | 4.5 | 4.5 | 4.5 | 4.5 | 4.5 |
| Total Length L in | 24.5 | 24.5 | 24.5 | 24.5 | 24.5 |

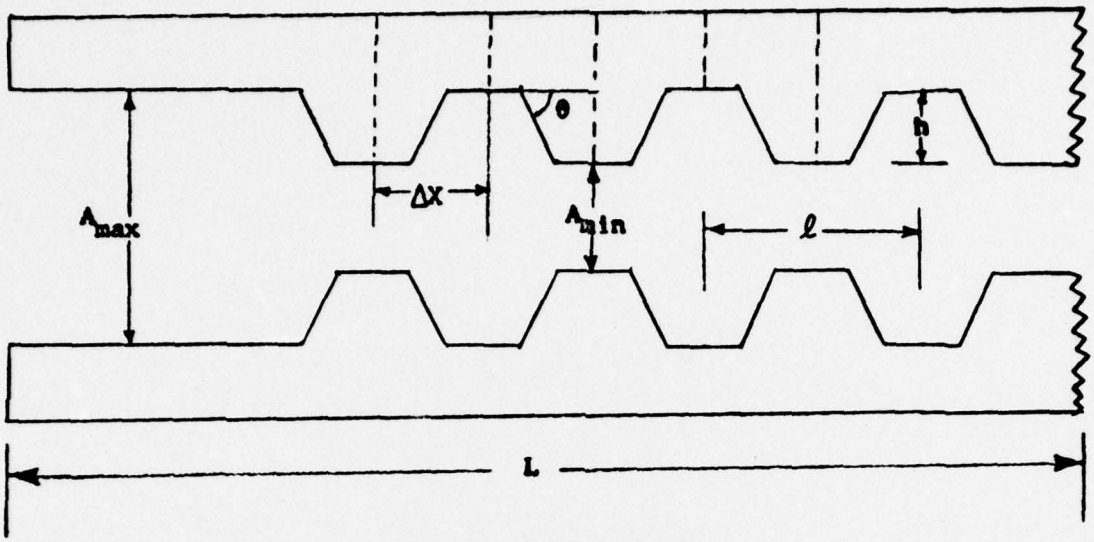


(a) Models A thru D

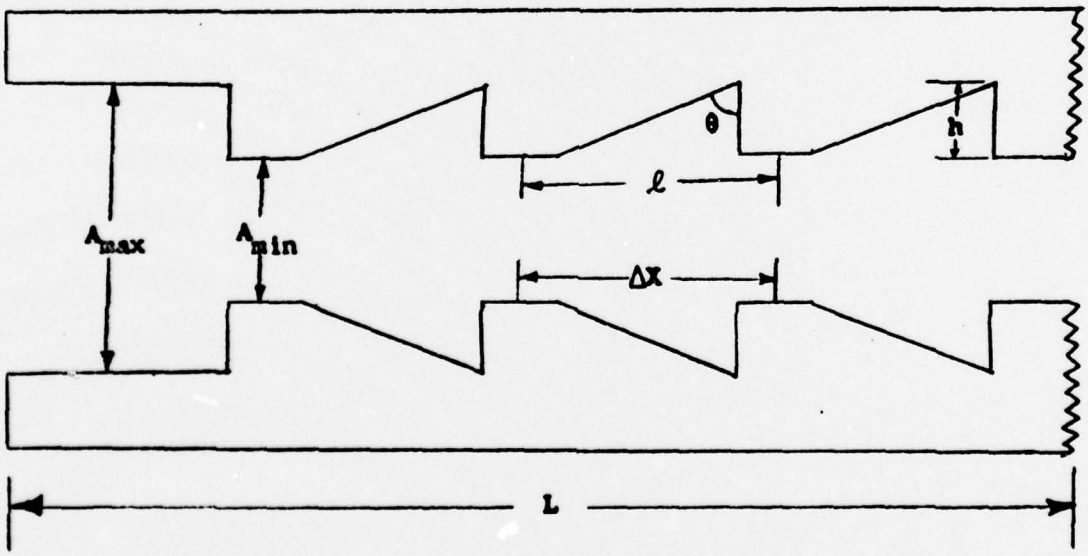


(b) Model E

Fig. 13 . Shapes and Nomenclature of Wall Shapes

## Appendix B

## Data Reduction Method

### Adjustment of Driver and Driven Pressure

Atmospheric pressure and temperature were recorded before the runs. Typical values were as follows:

$P_a$ = 29.22 inch Hg absolute

$T_a$ = 78° F.

The driven gas pressure $P_1$ was measured by a mercury manometer and was adjusted by means of the vacuum pump by-pass to achieve the desired pressure ratio as explained below:

Manometer Reading = -(10 + 9.75) = -19.75 inch Hg gauge

$P_1$ = (29.22 - 19.75) = 9.47 inch Hg absolute

Desired Pressure Ratio = 10

$P_4$ required = (10)(9.47) = 94.7 inch Hg absolute

= (94.7 - 29.22) = 65.48 inch Hg gauge

$P_4$ was measured by a dial gauge which overread slightly.

Dial Correction Factor = $\frac{P_{dial}}{P_{actual}}$ = 0.997

$P_4$ corrected = (65.48)(0.997) = 65.28 inch Hg gauge.

### Wave Speed Measurement by Using Pressure Transducers

The wave speed is defined as:

$$V = \frac{\Delta x}{\Delta t}$$

where

$\Delta x$ = Distance between two transducers.

$\Delta t$ = Average time taken by the wave to travel $\Delta x$, measured by means of the time interval counters.

The shock wave Mach number is defined as:

$$M = \frac{V}{a}$$

where

$a$ = Speed of Sound = $(\gamma RT)^{\frac{1}{2}}$,

$T$ = Temperature in deg Rankine.

For air with $\gamma = 1.4$, $a = 49.01\sqrt{T}$.

Wave Speed Measurement by Using Schlieren Optical System

Using the spark schlieren system, the delay time for the spark lamp firing signal could be varied for each run. This caused a corresponding shift in the position of the disturbance on the photograph. Utilizing the same reference pressure transducer, the difference between the two delay times gave the time disturbance needs to travel the known distance on the photograph. The speed of the disturbance was then determined as:

$$V = \frac{\Delta x}{\Delta t} \text{ (scale factor)}$$

where

$\Delta x$ = Distance traveled by the disturbance on the schlieren photograph.

$\Delta t$ = Difference between the two corresponding delay time settings.

The scale factor accounts for the picture magnification due to optics.

## Appendix C

## Reduced Tabular Data

Table II
Summary of Experimental Results for Disturbance
Attenuation in Irregular Duct
Model A $\theta = 0$ deg

| Transducers | Average Mach Number | Time Interval μ sec |
|---|---|---|
| A-B | 1.58 | 4841.5 |
| 1-2 | 1.92 | 749.7 |
| 2-3 | 2.03 | 72.2 |
| 3-4 | 1.65 | 178.3 |
| 4-5 | 1.37 | 107.3 |
| 5-6 | 2.32 | 63.2 |
| 6-7 | 1.77 | 83.1 |
| 7-8 | 1.27 | 116.3 |
| 8-9 | 1.76 | 83.5 |
| 9-10 | 1.69 | 87.1 |

Average Speed of Sound = 1133 ft/sec.

Table III
Summary of Experimental Results for Disturbance
Attenuation in Irregular Duct
Model B $\theta$ = 30 deg

| Transducers | Average Mach Number | Time Interval $\mu$ sec |
|---|---|---|
| A-B | 1.65 | 4608.3 |
| 1-2 | 1.96 | 580.0 |
| 2-3 | 0.85 | 520.4 |
| 3-4 | 1.95 | 150.9 |
| 4-5 | 1.16 | 125.7 |
| 5-6 | 0.63 | 234.3 |
| 6-7 | 1.67 | 87.8 |
| 7-8 | 2.06 | 71.3 |
| 8-9 | 1.28 | 114.3 |
| 9-10 | 2.75 | 53.2 |

Average Speed of Sound = 1137 ft/sec.

Table IV
Summary of Experimental Results for Disturbance
Attenuation in Irregular Duct
Model C $\theta$ = 60 deg

| Transducers | Average Mach Number | Time Interval $\mu$ sec |
|---|---|---|
| A-B | 1.62 | 4710.4 |
| 1-2 | 1.93 | 741.7 |
| 2-3 | 1.84 | 79.9 |
| 3-4 | 2.13 | 138.3 |
| 4-5 | 1.17 | 125.6 |
| 5-6 | 2.31 | 63.9 |
| 6-7 | 1.17 | 126.8 |
| 7-8 | 2.4 | 62.0 |
| 8-9 | 0.74 | 198.5 |
| 9-10 | 1.41 | 104.7 |

Average Speed of Sound = 1133 ft/sec.

Table V
Summary of Experimental Results for Disturbance Attenuation in Irregular Duct
Model D $\theta$ = 90 deg

| Transducers | Average Mach Number | Time Interval μ sec |
|---|---|---|
| A-B | 1.58 | 4820.1 |
| 1-2 | 1.92 | 745.1 |
| 2-3 | 2.32 | 65.8 |
| 3-4 | 1.71 | 171.7 |
| 4-5 | 1.29 | 113.6 |
| 5-6 | 1.02 | 143.2 |
| 6-7 | 1.36 | 108.0 |
| 7-8 | 0.48 | 305.9 |
| 8-9 | 0.42 | 349.2 |
| 9-10 | 0.46 | 317.9 |

Average Speed of Sound = 1136 ft/sec.

Table VI
Summary of Experimental Results for Disturbance
Attenuation in Irregular Duct
Model E $\theta$ = 63 deg

| Transducers | Average Mach Number | Time Interval $\mu$ sec |
|---|---|---|
| A-B | 1.55 | 4982.0 |
| 1-2 | 1.92 | 752.7 |
| 2-3 | 0.64 | 690.1 |
| 3-4 | 2.00 | 148.2 |
| 4-5 | 0.38 | 392.3 |
| 5-6 | 0.10 | 1954.9 |
| 6-7 | 1.43 | 103.6 |
| 7-8 | 1.47 | 101.1 |
| 8-9 | 0.20 | 830.0 |
| 9-10 | 0.81 | 182.7 |

Average Speed of Sound = 1124 ft/sec.

## Appendix D

## Schlieren Photographs of Flow Field Behind Shock Wave, Models B thru E

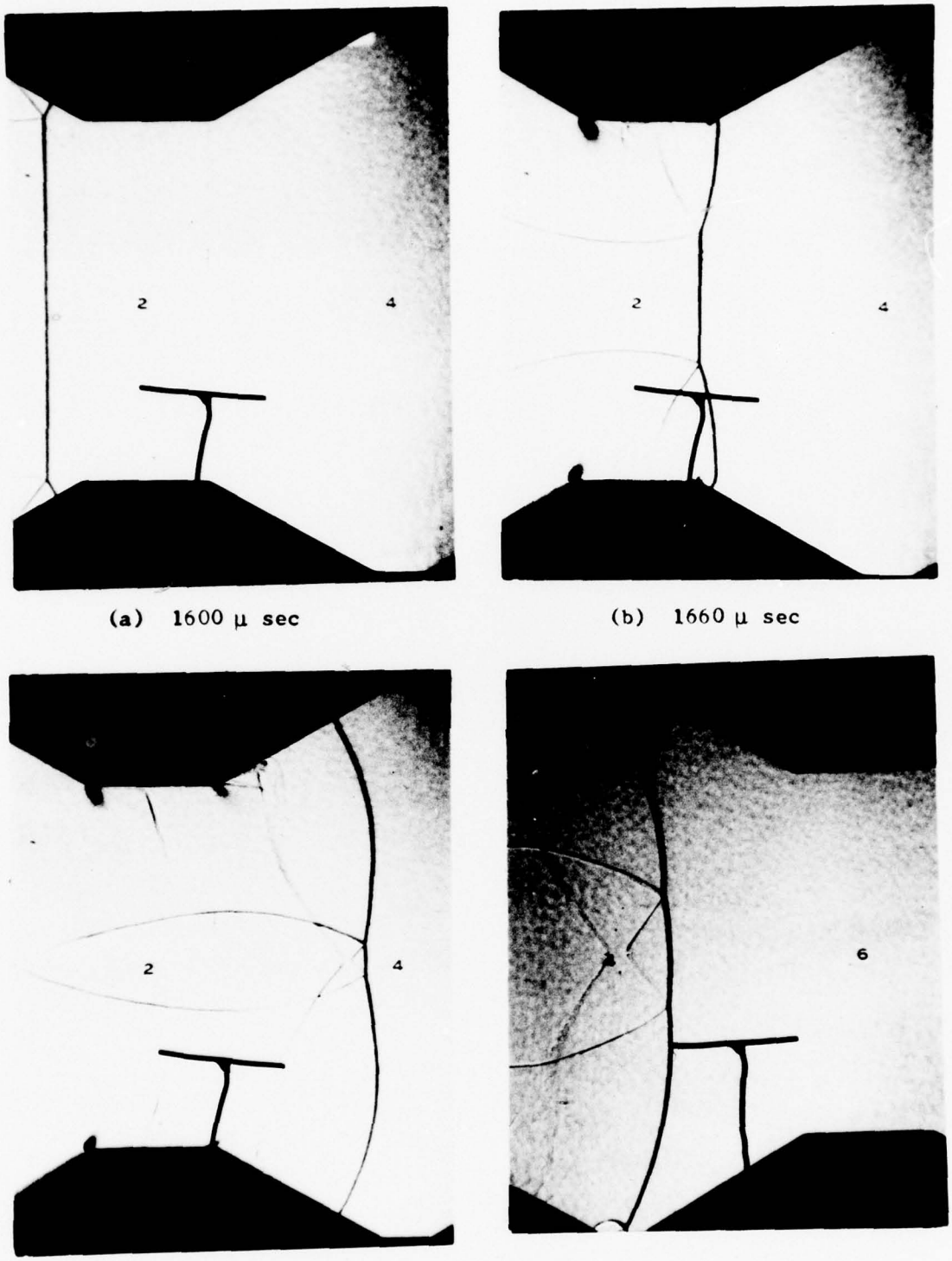


(a) 1600 μ sec

(b) 1660 μ sec

(c) 1680 μ sec

(d) 1700 μ sec

Fig. 14. Schlieren Photographs of Flow Field Behind Shock Wave, Model B, $\theta$ = 30 deg.

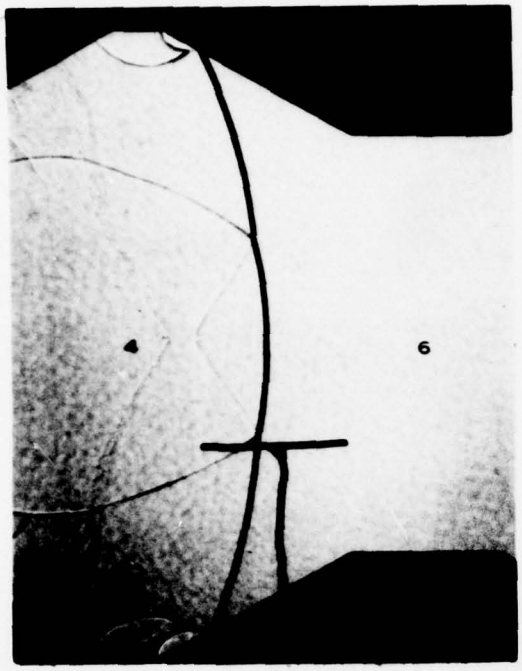

(e) 1700 μ sec

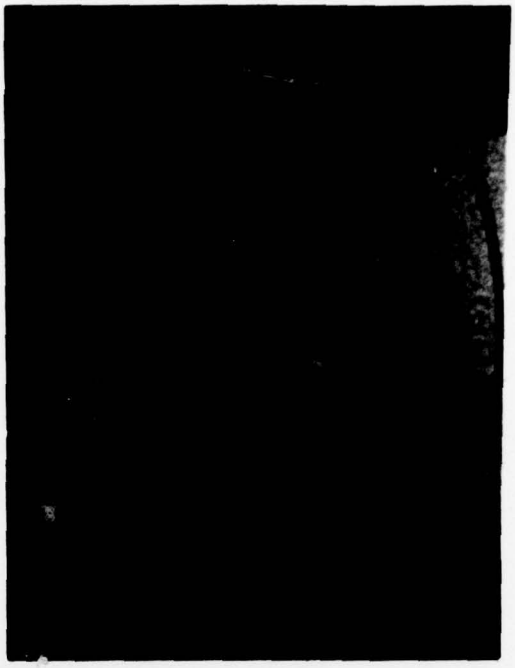

(f) 1750 μ sec

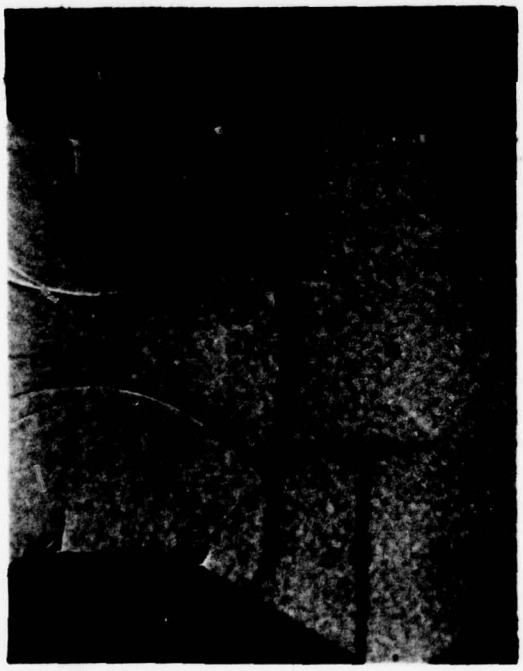

(g) 1870 μ sec

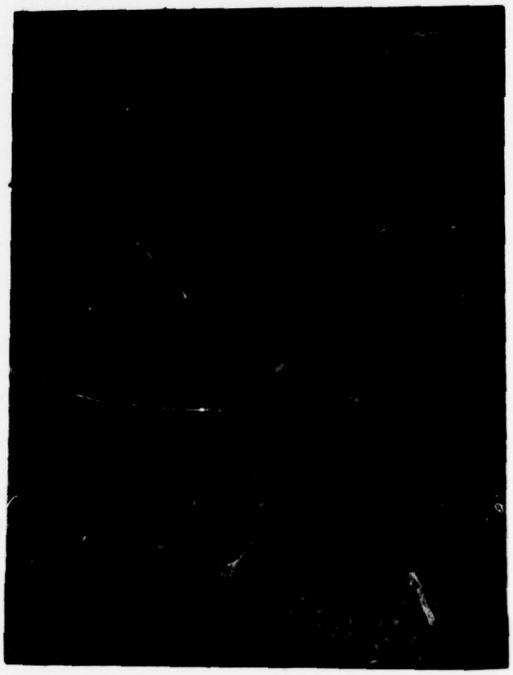

(h) 1900 μ sec

Fig. 14. (continued) Schlieren Photographs of Flow Field Behind Shock Wave, Model B, $\theta$ = 30 deg.

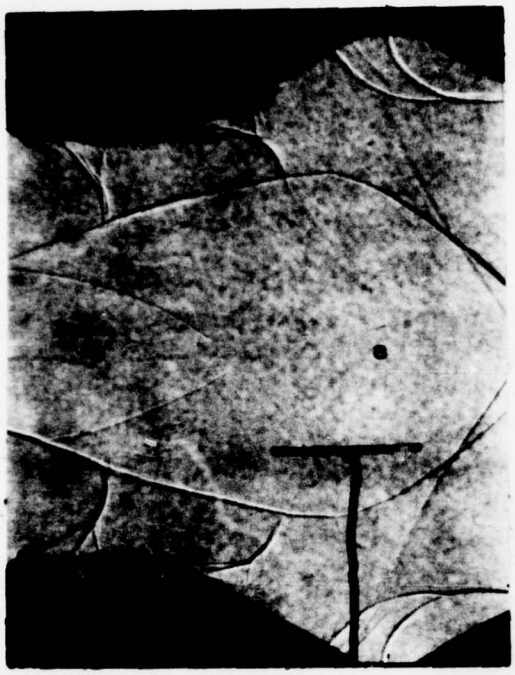

(i) 1930 μ sec

(j) 2020 μ sec

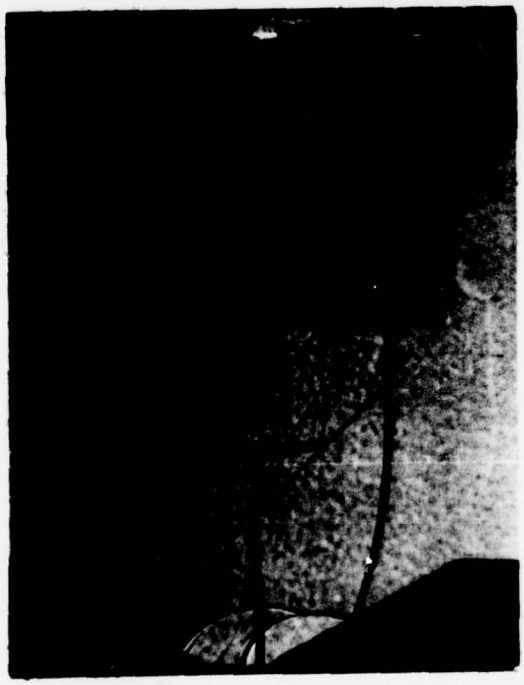

(k) 2040 μ sec

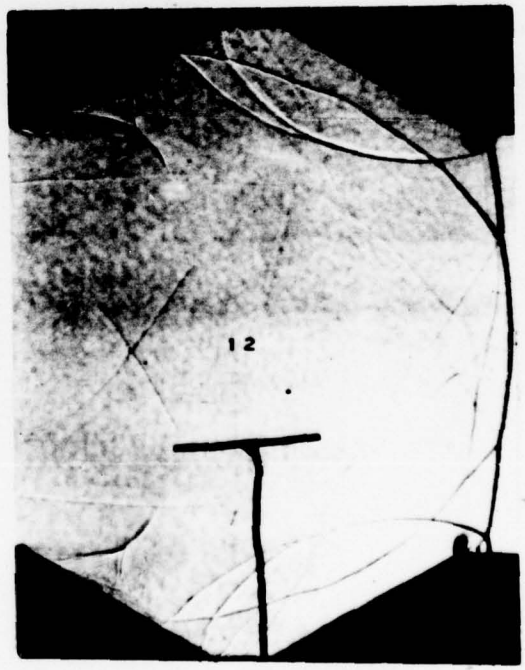


(l) 2070 μ sec

Fig. 14 . (continued) Schlieren Photographs of Flow Field Behind Shock Wave, Model B, $\theta$ = 30 deg.

(m) 2100 μ sec

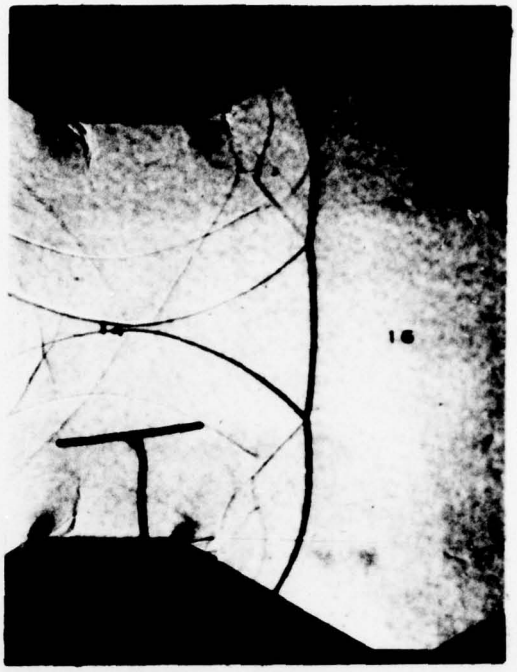

(n) 2160 μ sec

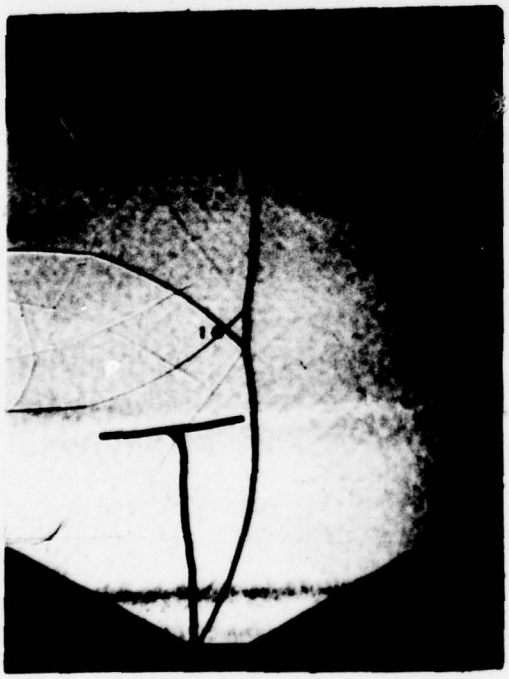

(o) 2200 μ sec

(p) 2240 μ sec

Fig. 14. (continued) Schlieren Photographs of Flow Field Behind Shock Wave, Model B, θ = 30 deg.

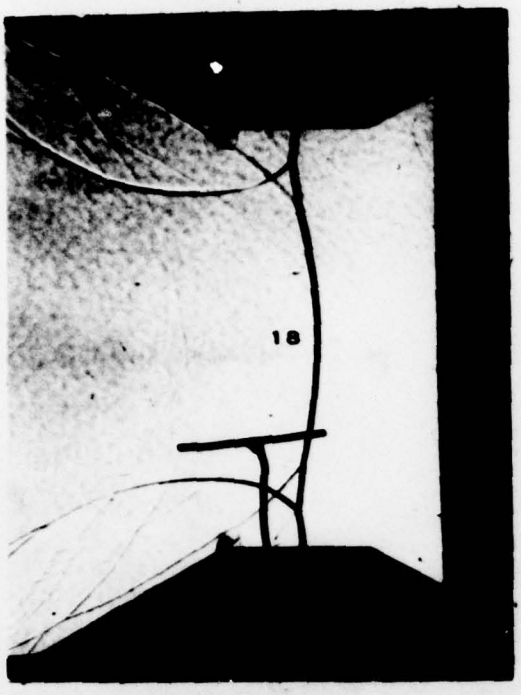

(q) 2260 μ sec

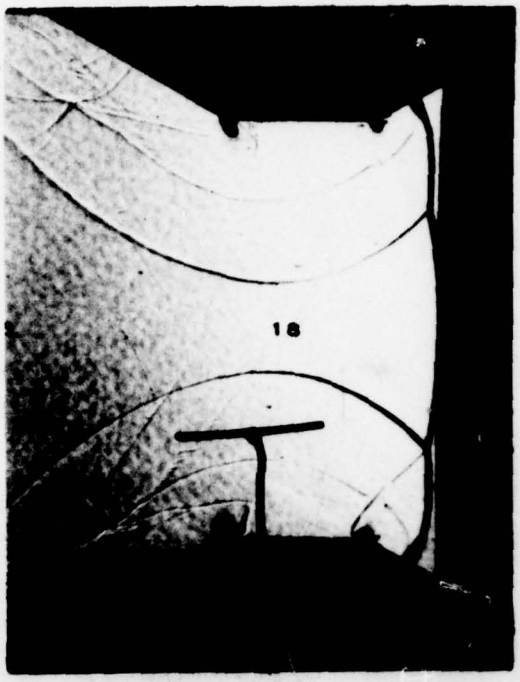

(r) 2280 μ sec

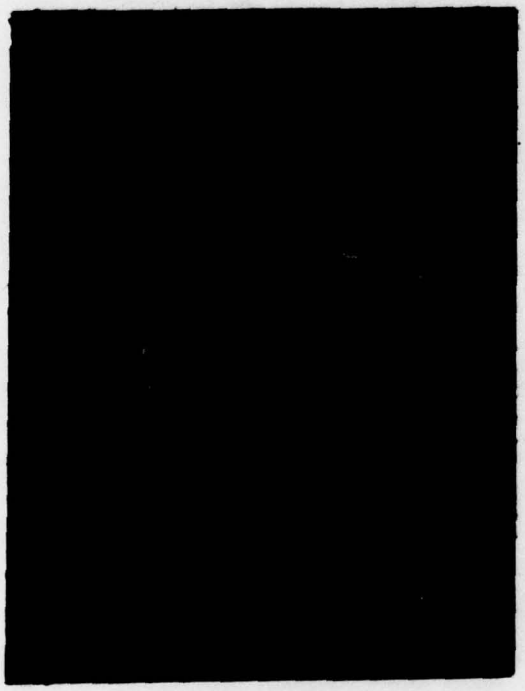

(s) 2300 μ sec

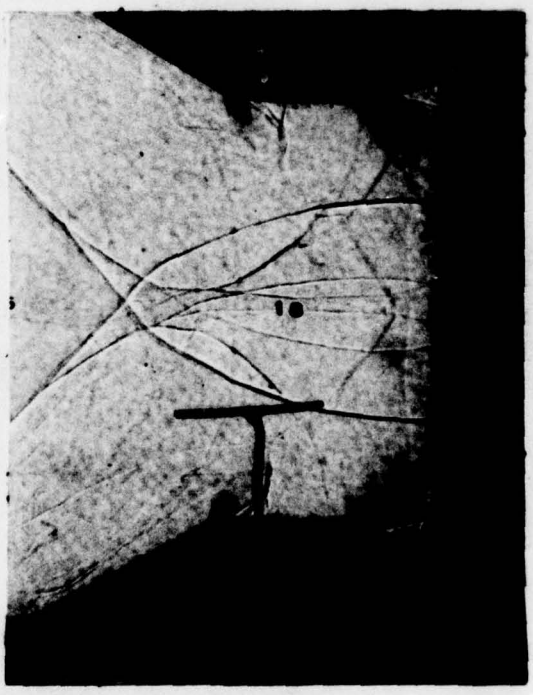

(t) 2360 μ sec

Fig. 14 . (continued) Schlieren Photographs of Flow Field Behind Shock Wave, Model B, θ = 30 deg.

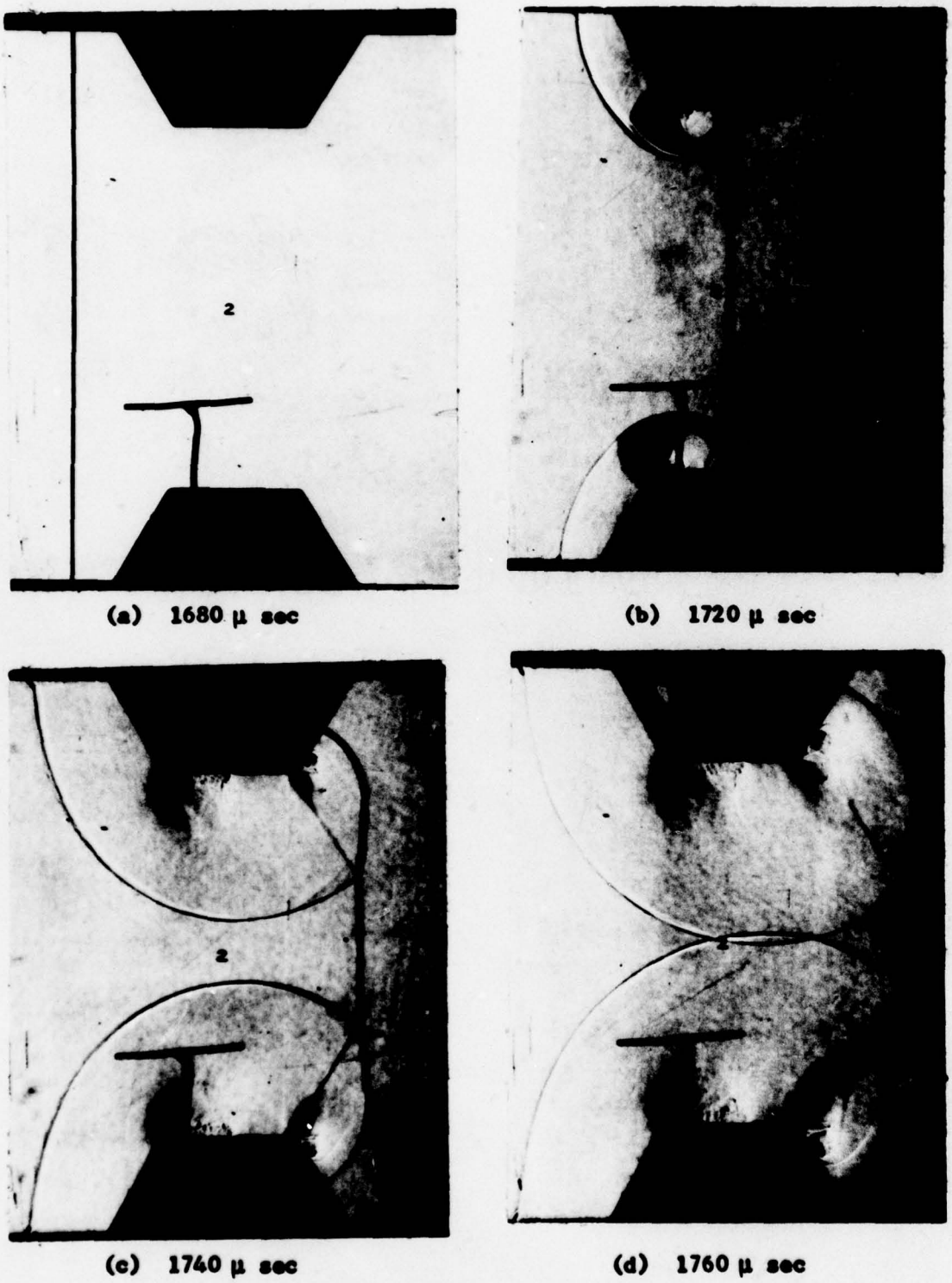


(a) 1680 μ sec

(b) 1720 μ sec

(c) 1740 μ sec

(d) 1760 μ sec

Fig. 15. Schlieren Photographs of Flow Field Behind Shock Wave, Model C, θ = 60 deg.

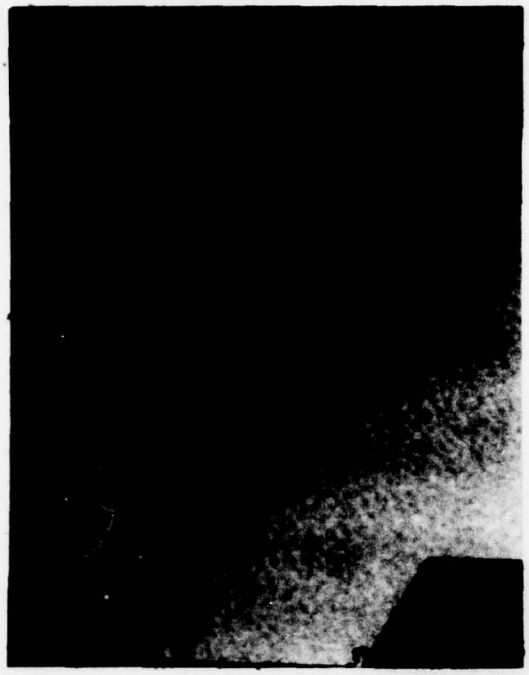

(e) 1770 μ sec

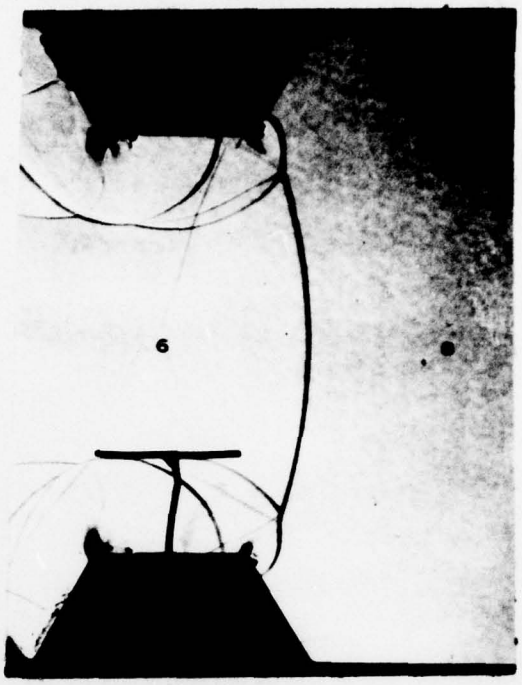

(f) 1800 μ sec

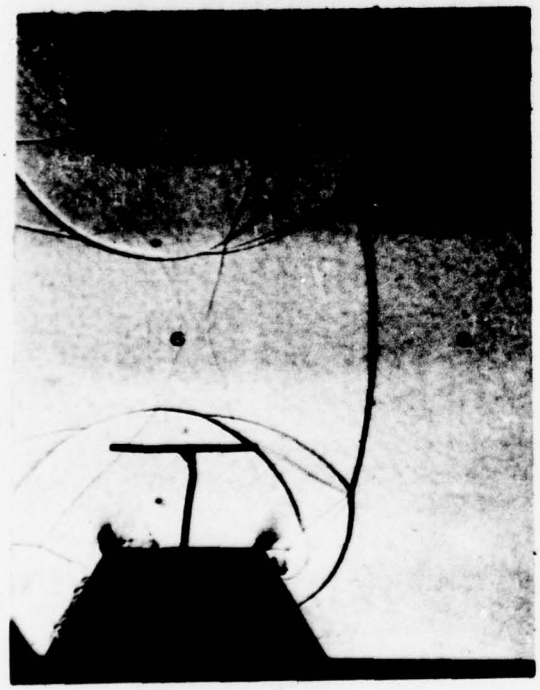

(g) 1820 μ sec

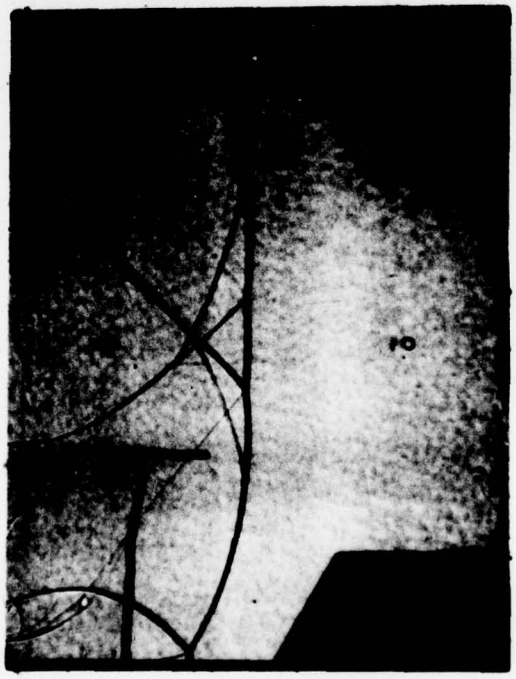

(h) 1900 μ sec

Fig. 15 . (continued) Schlieren Photographs of Flow Field Behind Shock Wave, Model C, θ = 60 deg.

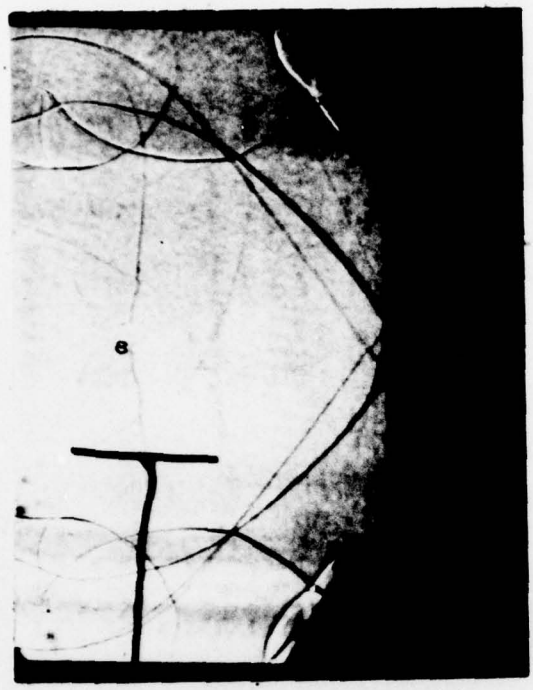

(i) 1960 μ sec

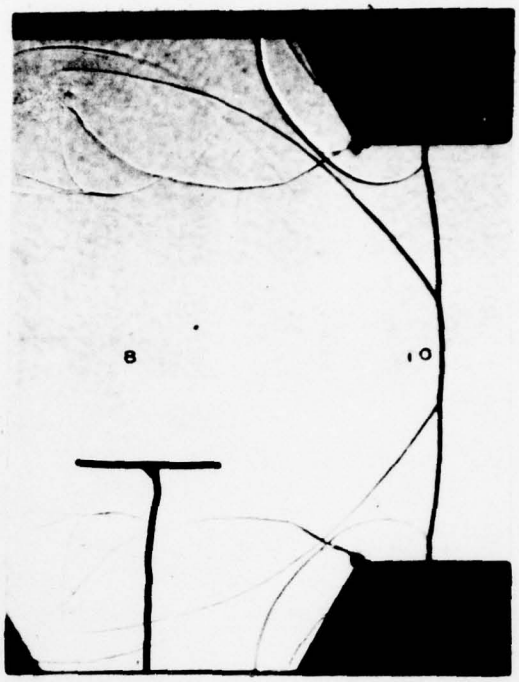

(j) 1965 μ sec

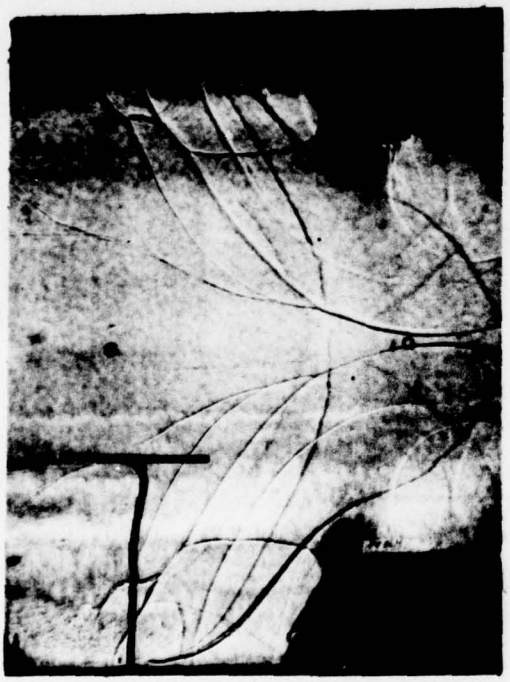

(k) 1970 μ sec

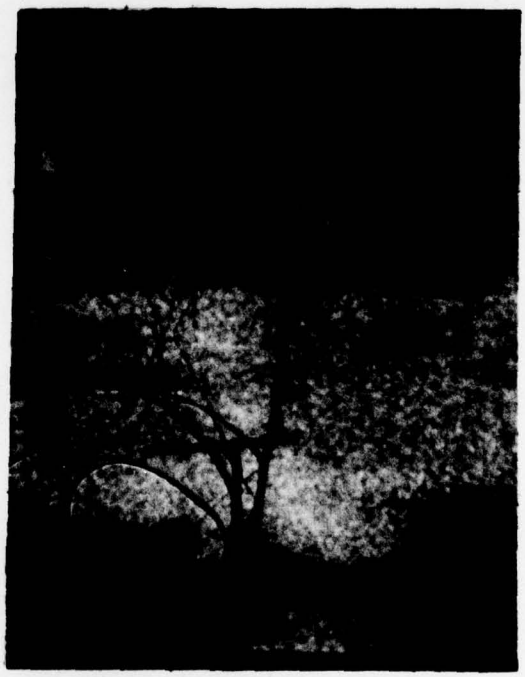

(l) 2030 μ sec

Fig. 15 . (continued) Schlieren Photographs of Flow Field Behind Shock Wave, Model C, $\theta$ = 60 deg.

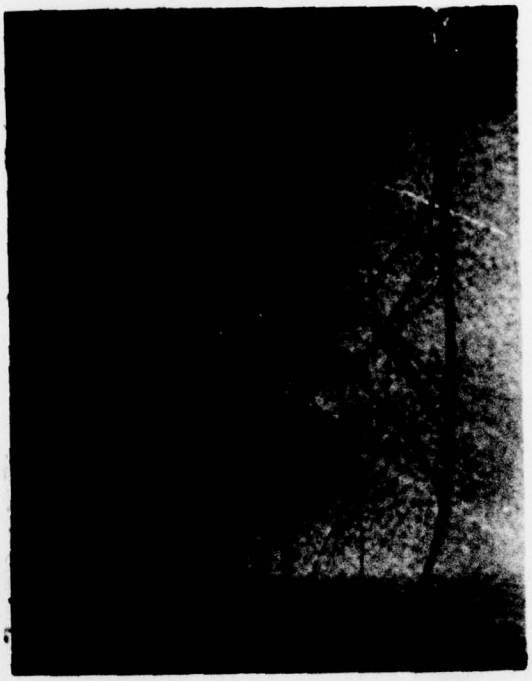

(m) 2080 μ sec

(n) 2090 μ sec

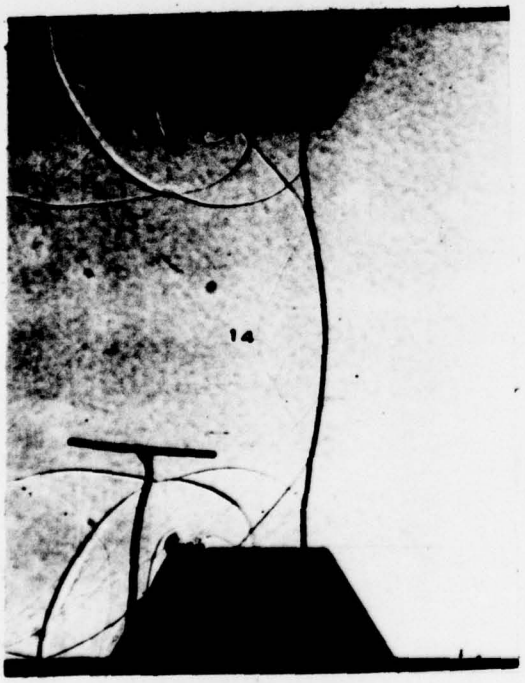

(o) 2130 μ sec

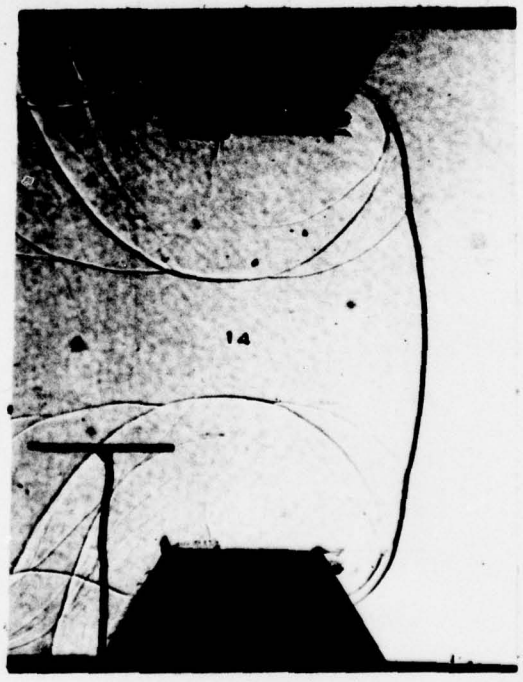

(p) 2190 μ sec

Fig. 15 . (continued) Schlieren Photographs of Flow Field Behind Shock Wave, Model C, θ = 60 deg.

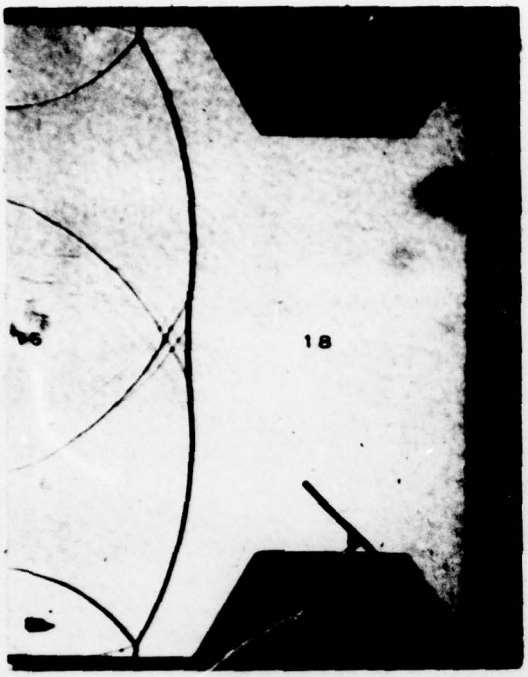


(q) 2270 μ sec

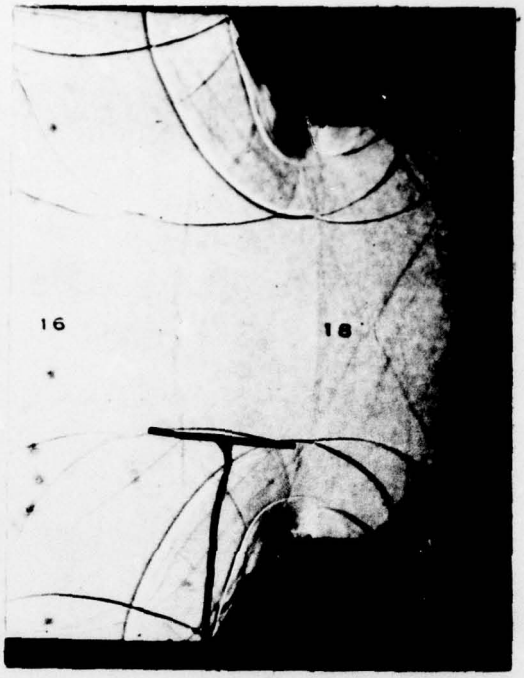


(r) 2450 μ sec

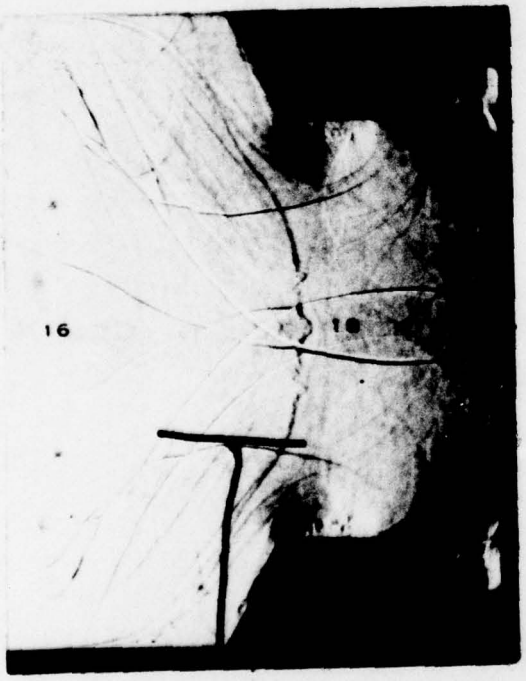


(s) 2500 μ sec

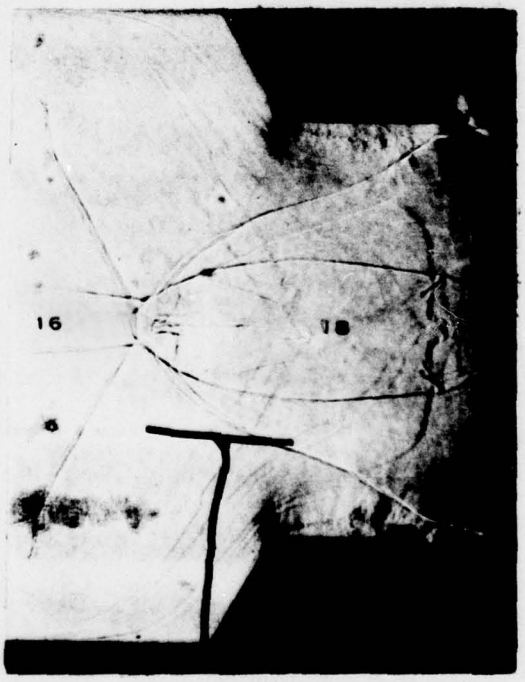


(t) 2550 μ sec

Fig. 15. (continued) Schlieren Photographs of Flow Field Behind Shock Wave, Model C, θ = 60 deg.

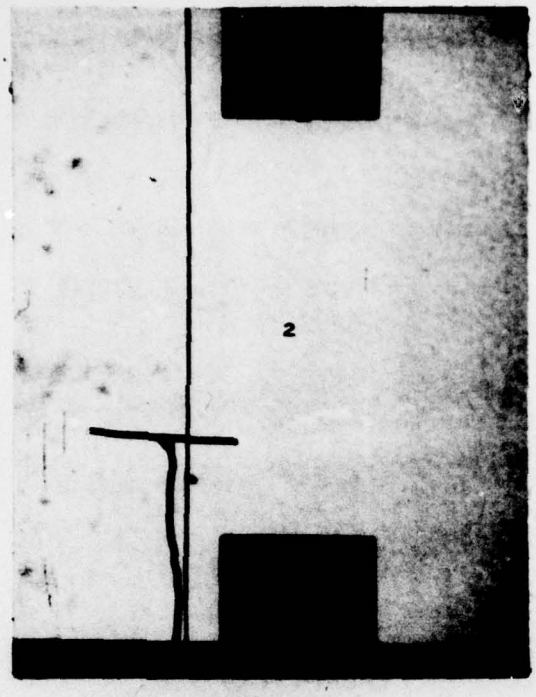

(a) 1670 μ sec

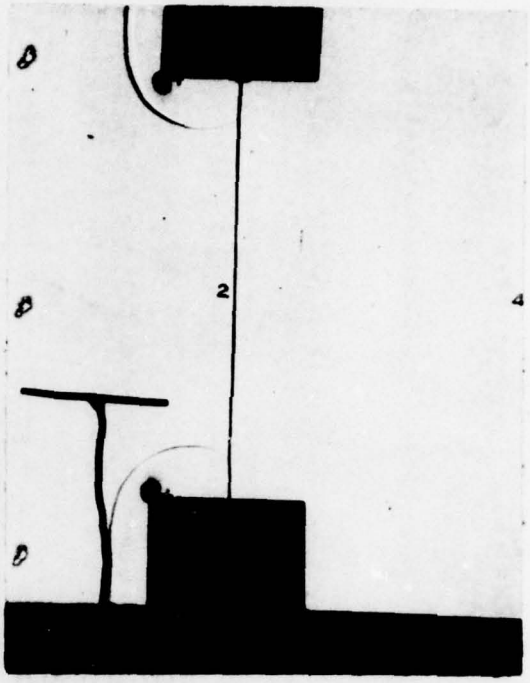

(b) 1700 μ sec

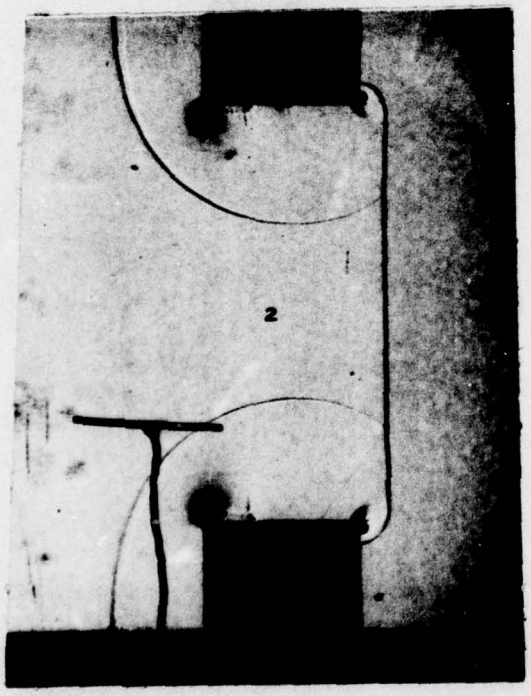

(c) 1740 μ sec

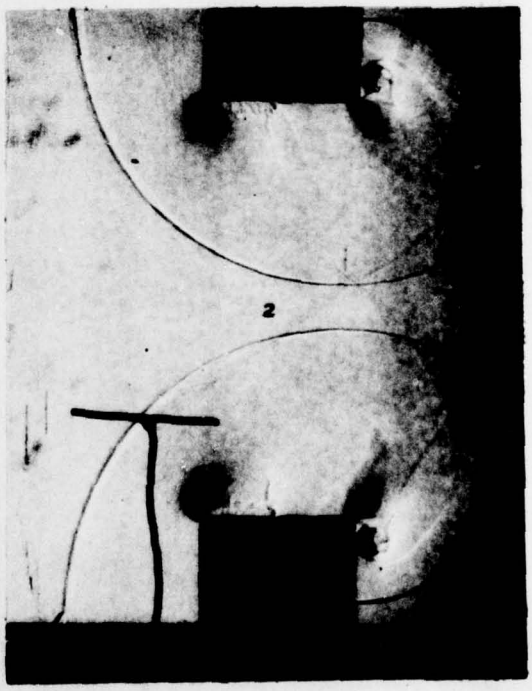

(d) 1760 μ sec

Fig. 16 . Schlieren Photographs of Flow Field Behind Shock Wave, Model D, θ = 90 deg.

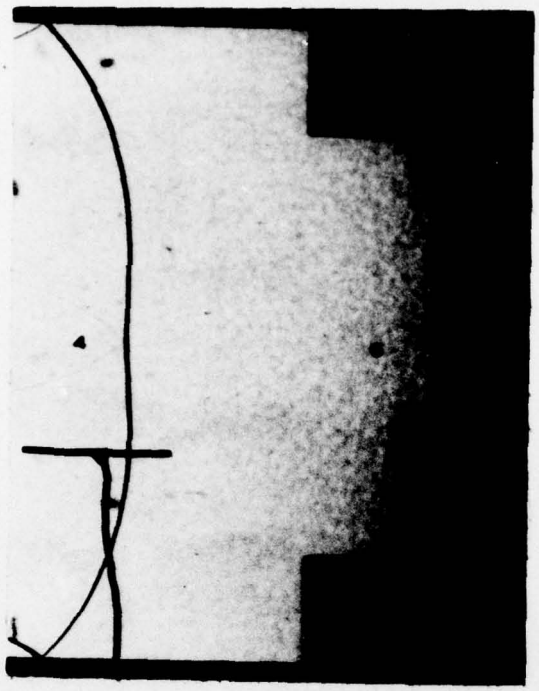

(e) 1810 μ sec

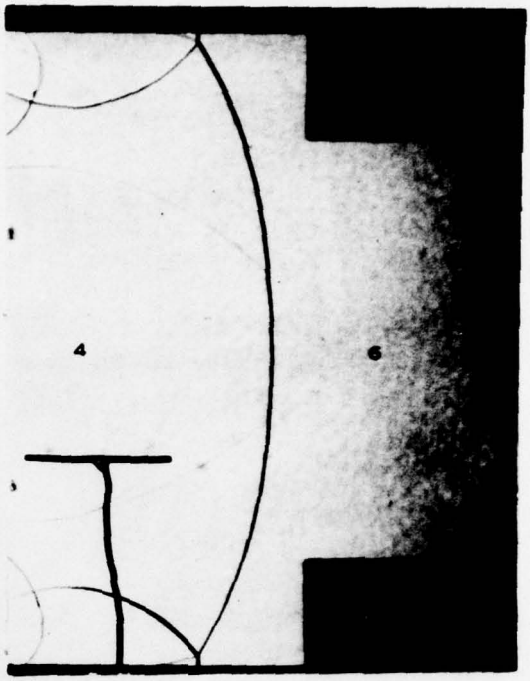

(f) 1840 μ sec

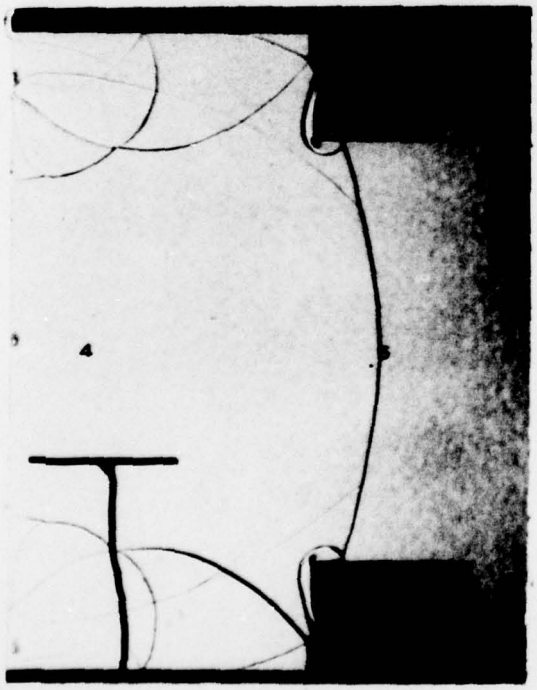

(g) 1870 μ sec

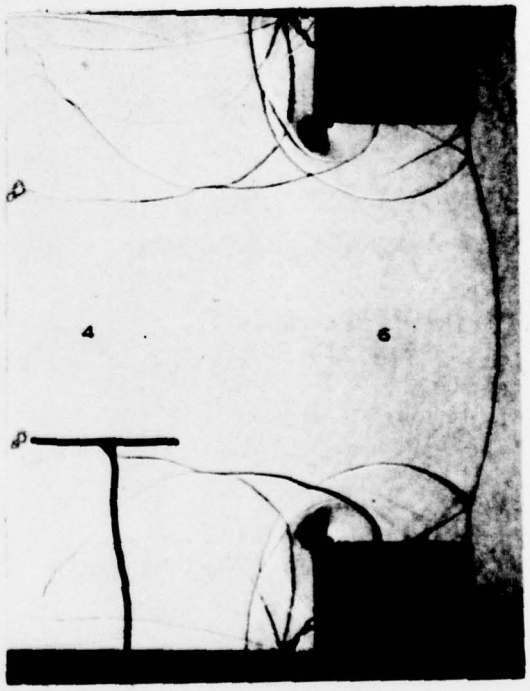

(h) 1900 μ sec

Fig. 16. (continued) Schlieren Photographs of Flow Field Behind Shock Wave, Model D, $\theta$ = 90 deg.

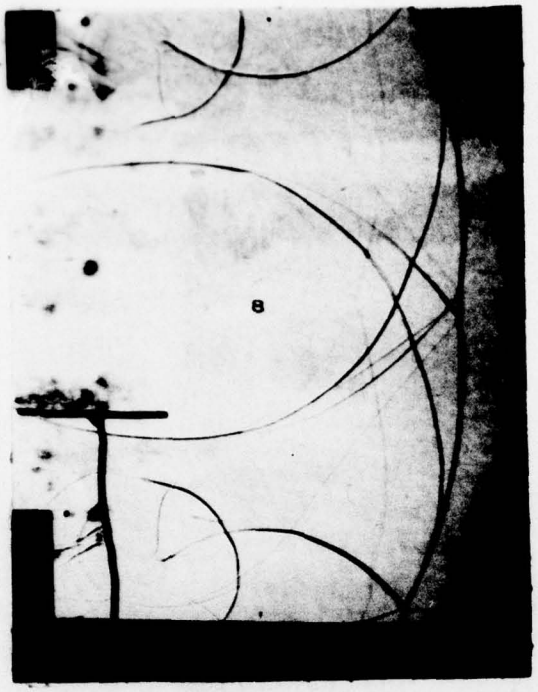

(i) 2020 μ sec

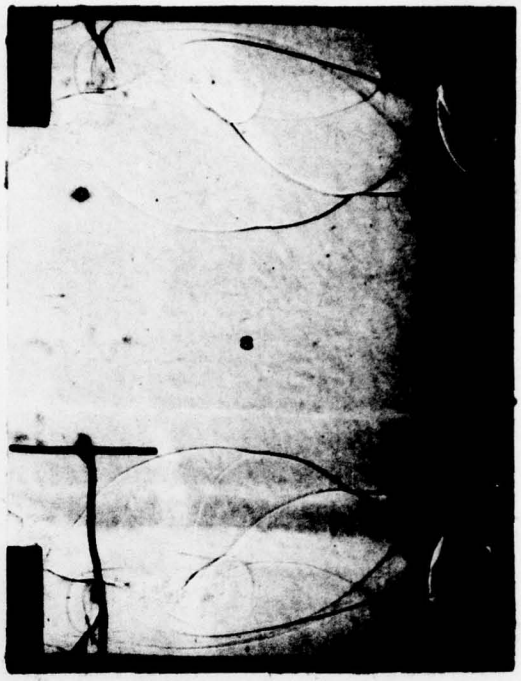

(j) 2040 μ sec

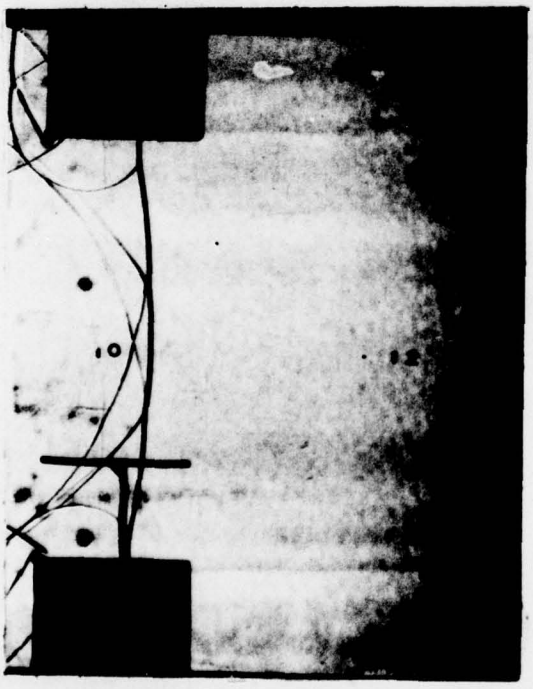

(k) 2060 μ sec

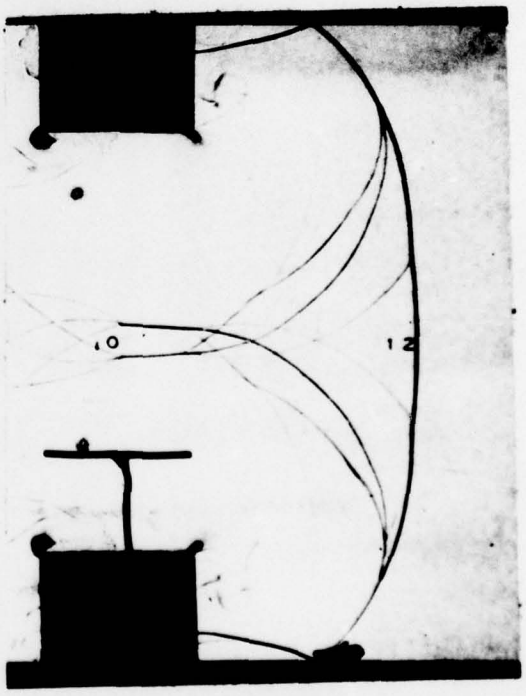

(l) 2170 μ sec

Fig. 16. (continued) Schlieren Photographs of Flow Field Behind Shock Wave, Model D, $\theta$ = 90 deg.

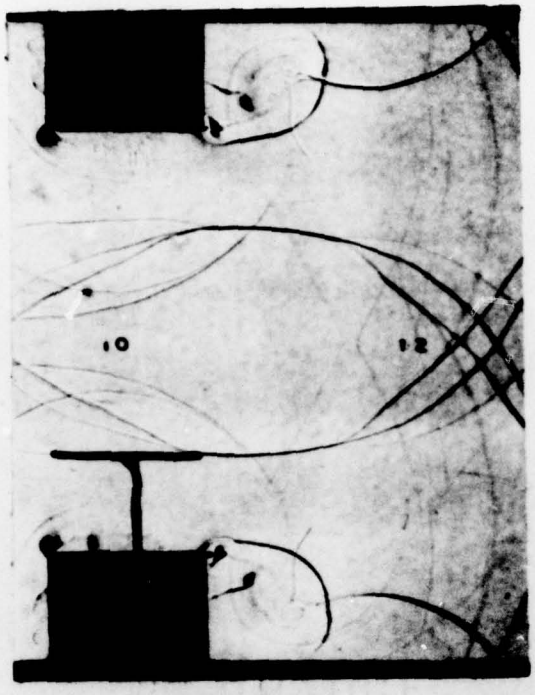

(m) 2170 μ sec

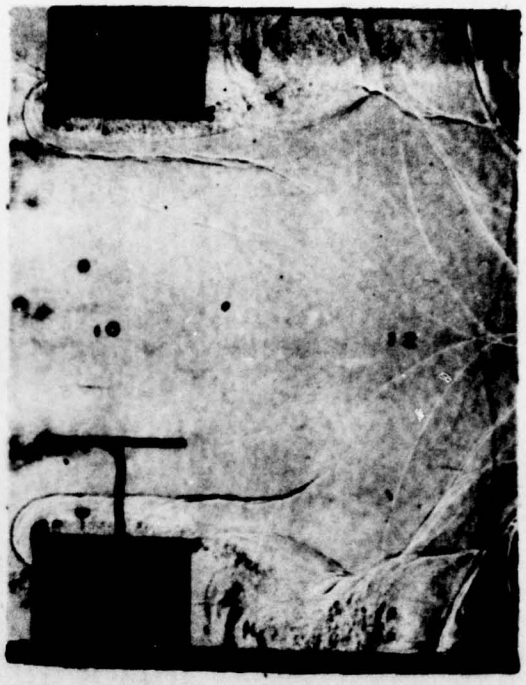

(n) 2280 μ sec

(o) 2320 μ sec

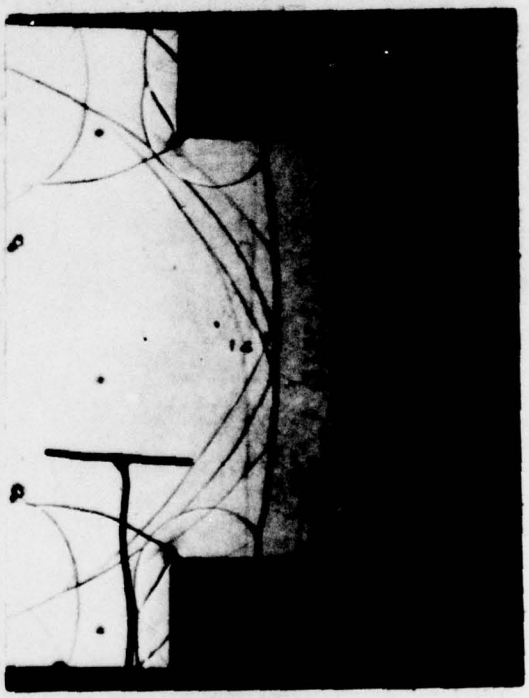

(p) 2210 μ sec

Fig. 16 . (continued) Schlieren Photographs of Flow Field Behind Shock Wave, Model *D*, $\theta = 90$ deg.

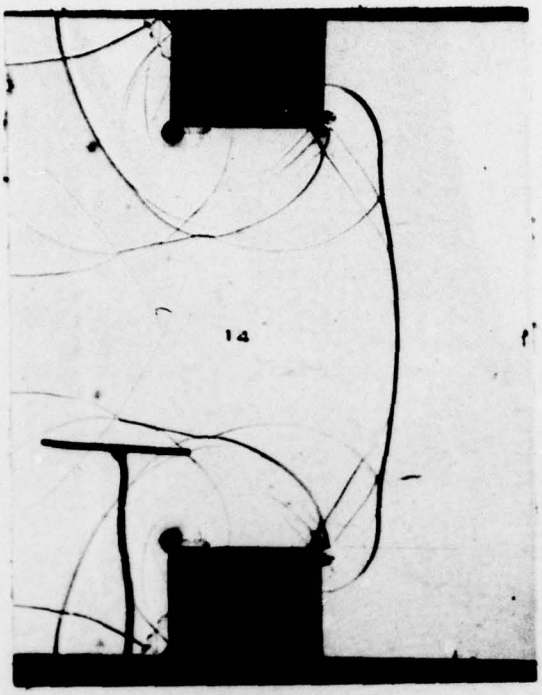


(q) 2260 μ sec

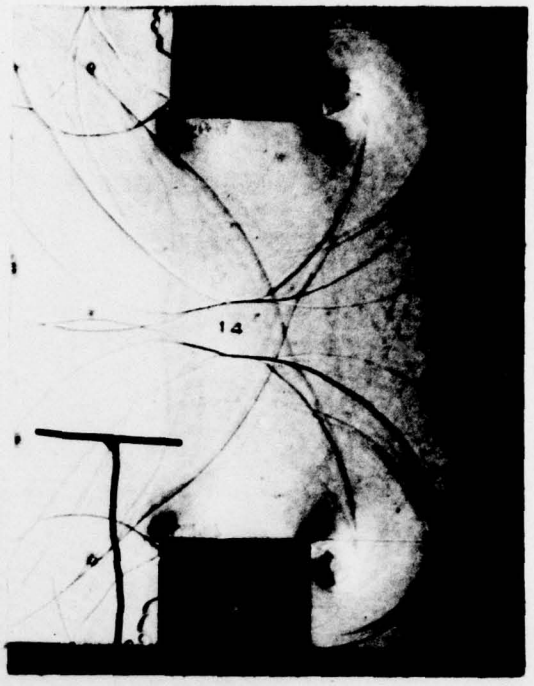


(r) 2290 μ sec

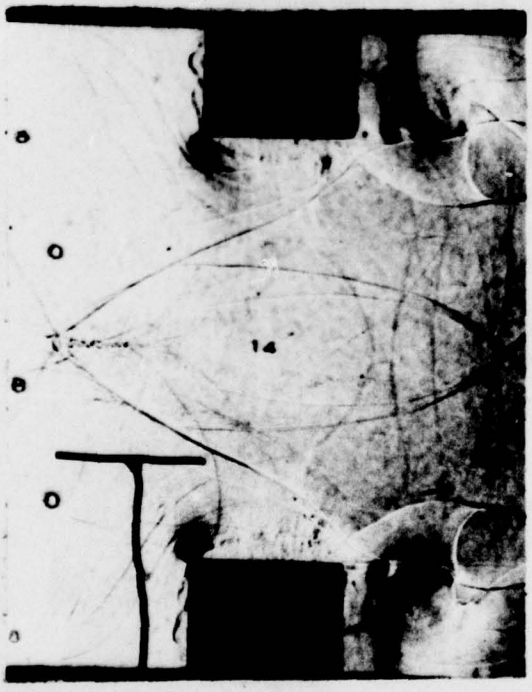


(s) 2380 μ sec

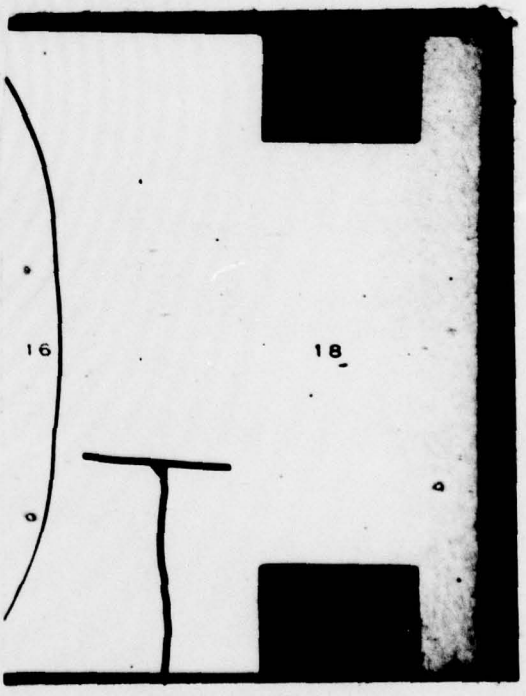


(t) 2350 μ sec

Fig. 16. (continued) Schlieren Photographs of Flow Field Behind Shock Wave, Model D, θ = 90 deg.

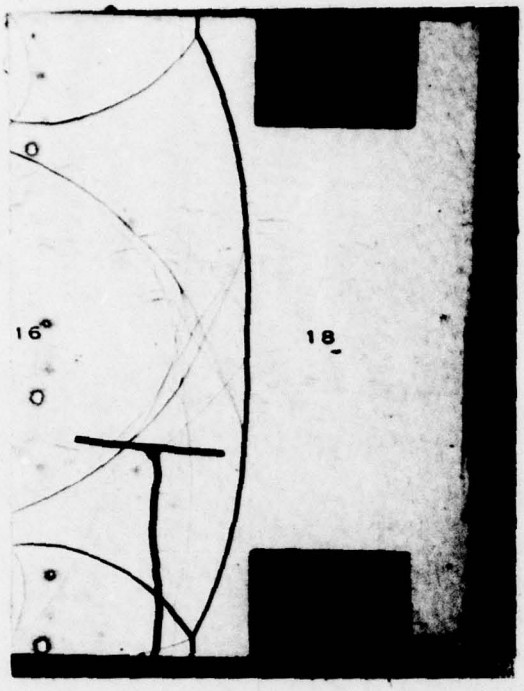


(u) 2390 μ sec

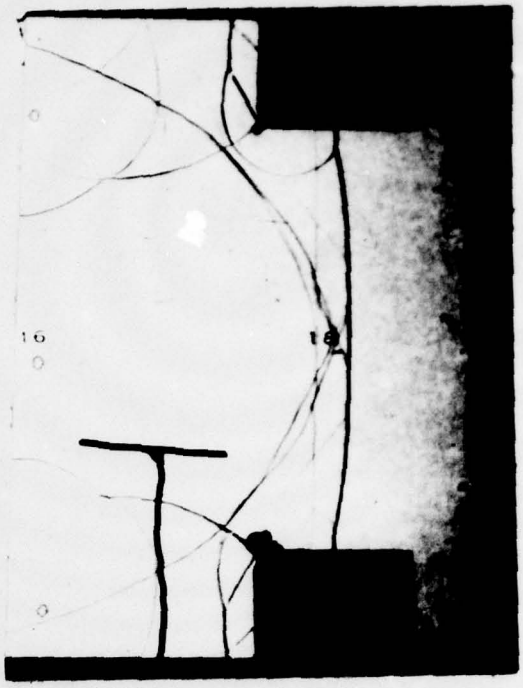


(v) 2430 μ sec


(w) 2440 μ sec

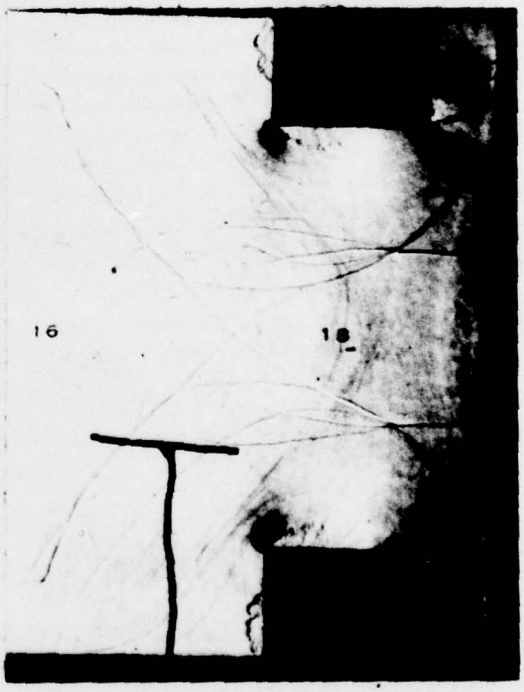


(x) 2520 μ sec

Fig. 16. (continued) Schlieren Photographs of Flow Field Behind Shock Wave, Model D, θ = 90 deg.

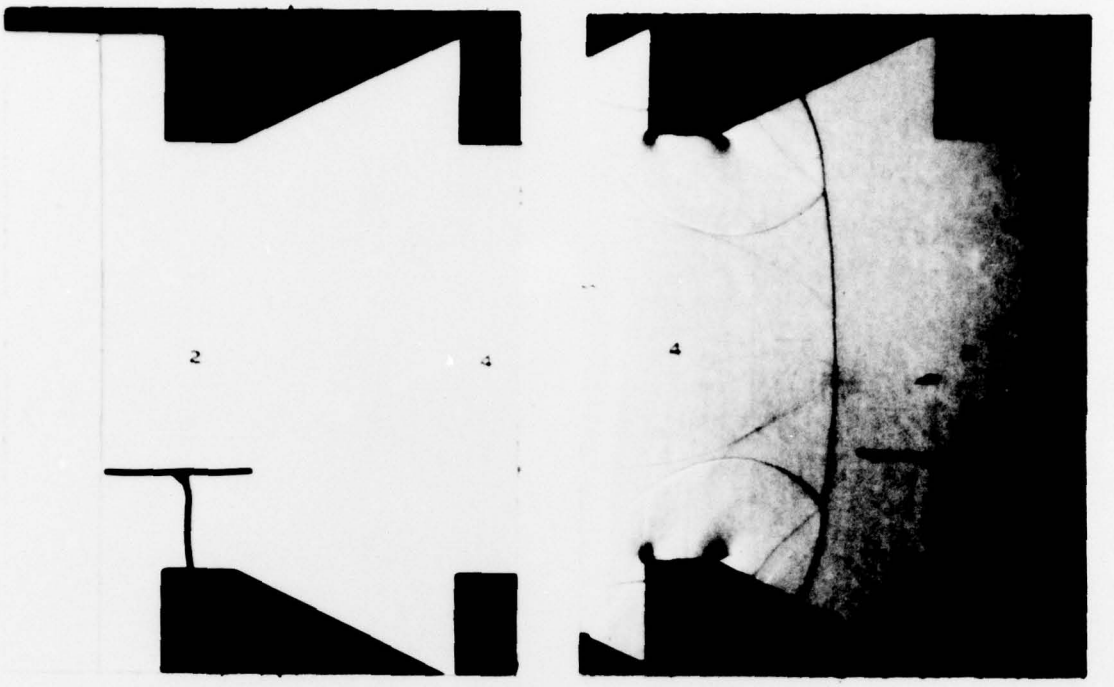

(a) 1770 μ sec

(b) 1900 μ sec

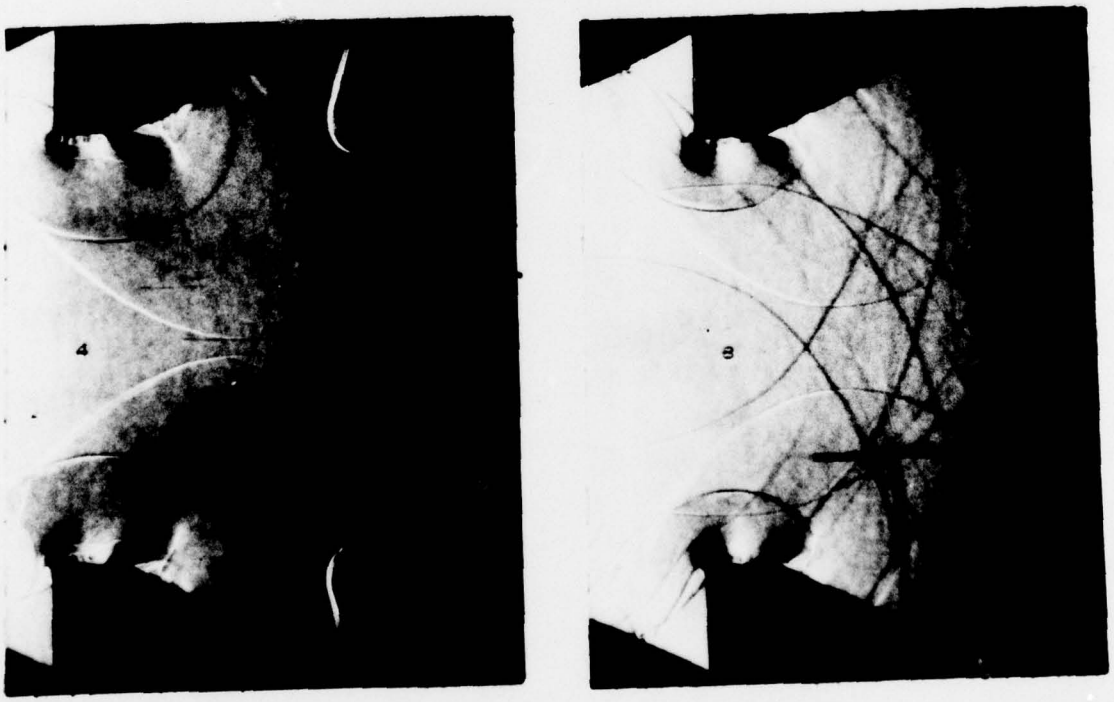

(c) 1930 μ sec

(d) 2080 μ sec

Fig. 17. Schlieren Photographs of Flow Field Behind Shock Wave, Model E, θ = 63 deg.

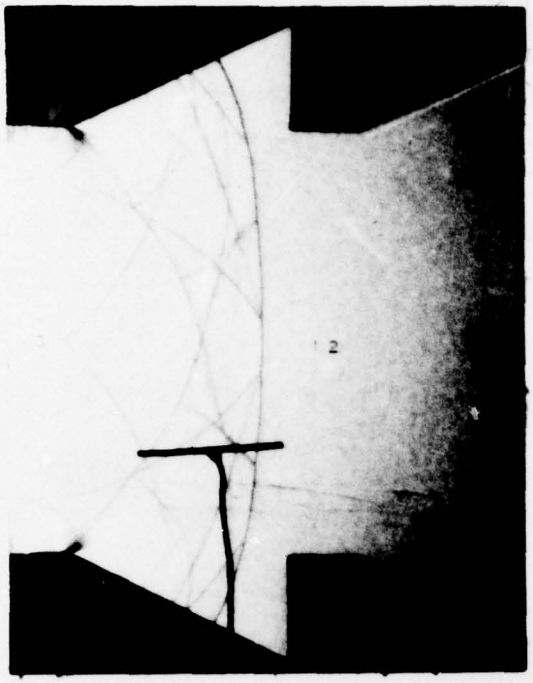

(e) 2170 μ sec

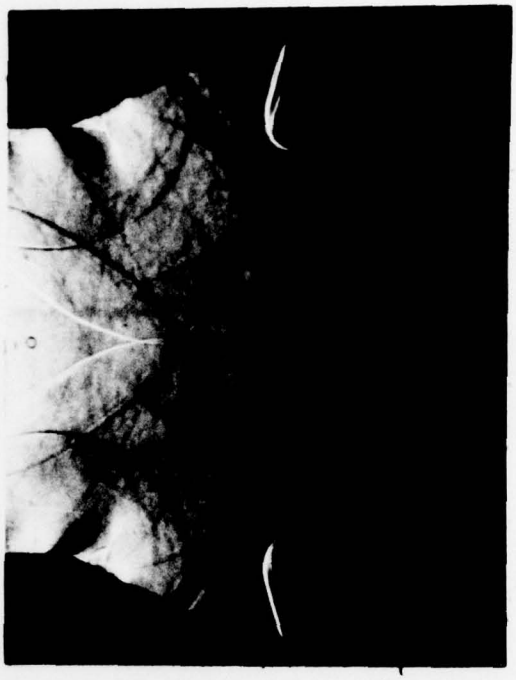

(f) 2180 μ sec

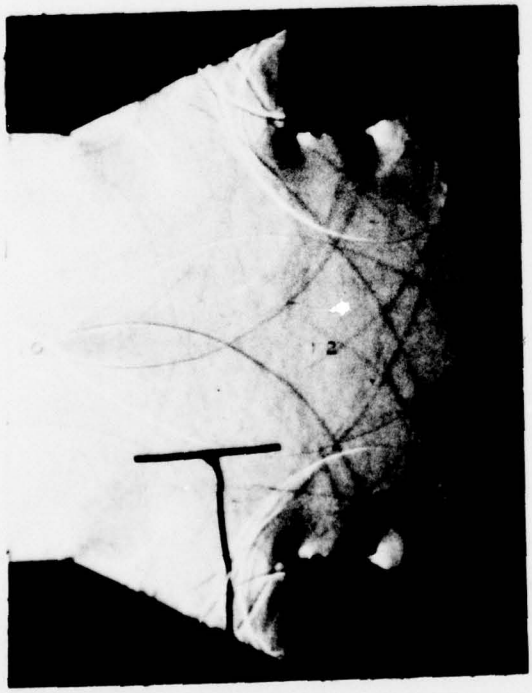

(g) 2220 μ sec

(h) 2270 μ sec

Fig. 17. (continued) Schlieren Photographs of Flow Field Behind Shock Wave, Model E, θ = 63 deg.

(i) 2330 μ sec

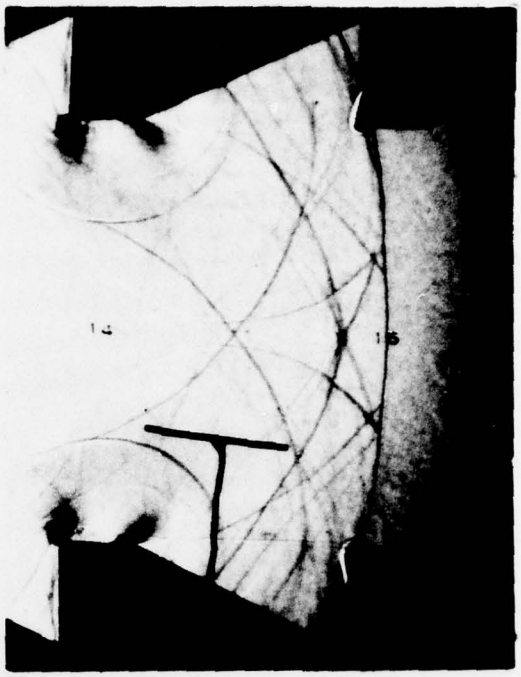

(j) 2360 μ sec

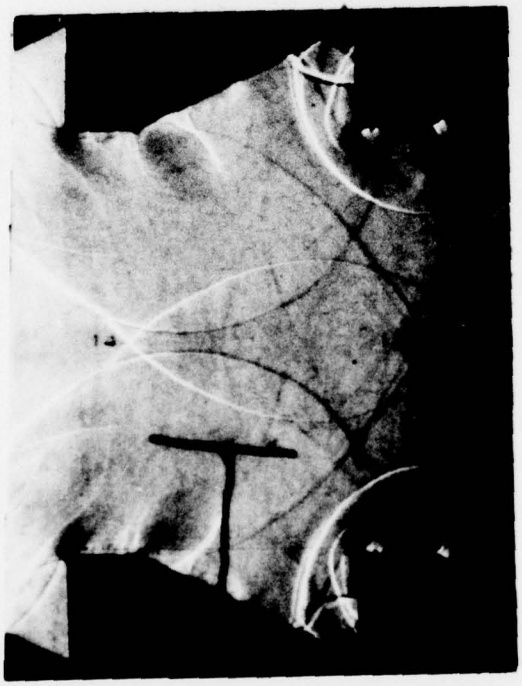

(k) 2400 μ sec

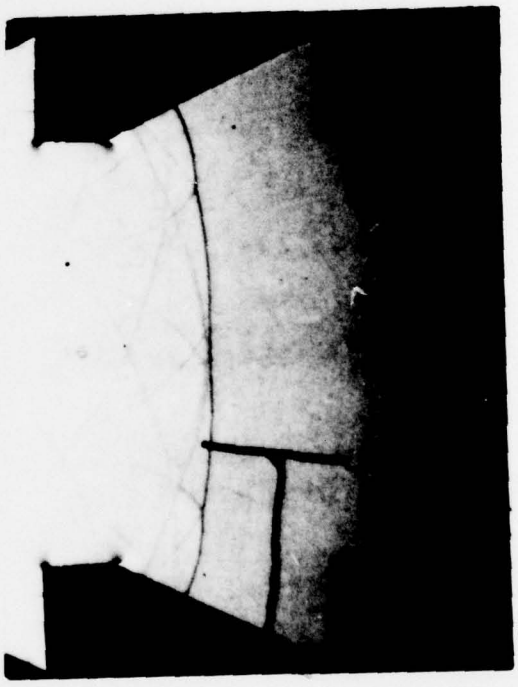

(l) 2430 μ sec

Fig. 17. (continued) Schlieren Photographs of Flow Field Behind Shock Wave, Model E, $\theta$ = 63 deg.

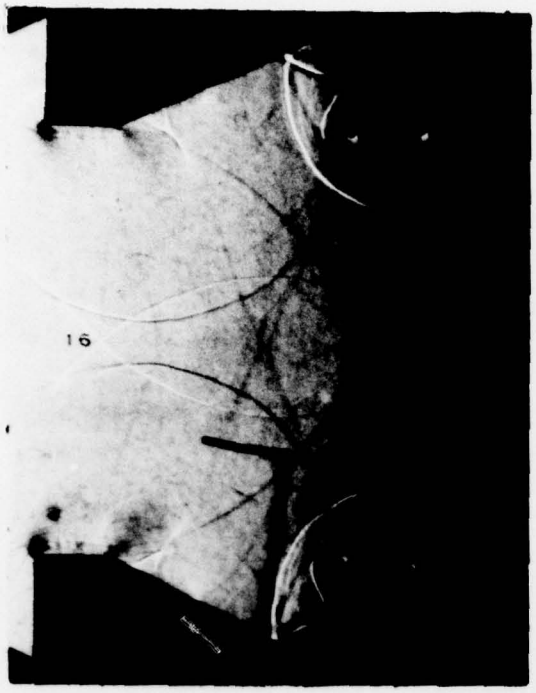


(m) 2530 μ sec

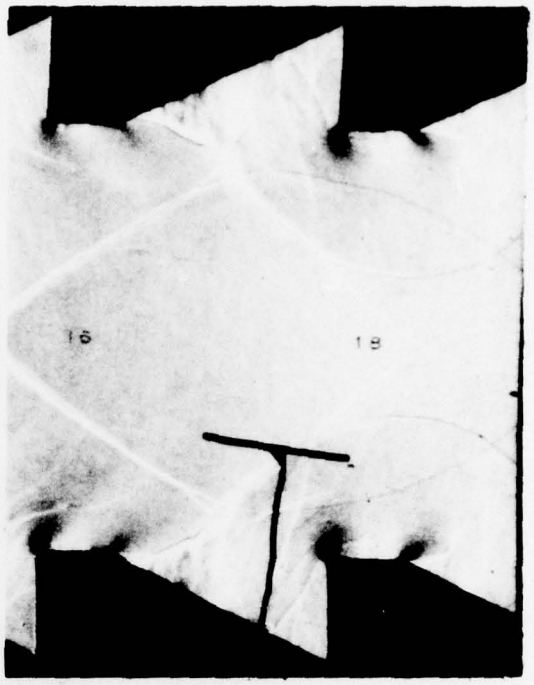


(n) 2600 μ sec

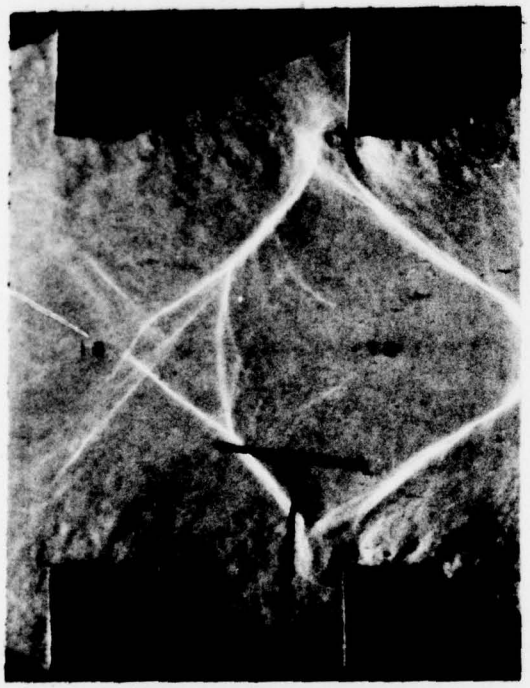

(o) 2800 μ sec

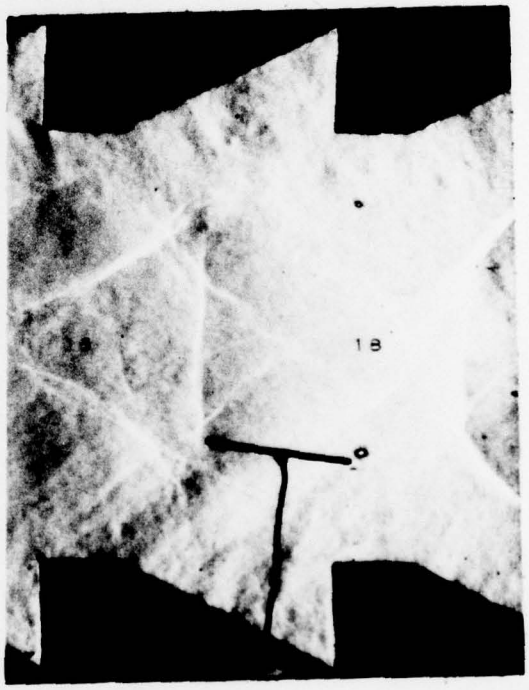


(p) 2900 μ sec

Fig. 17. (continued) Schlieren Photographs of Flow Field Behind Shock Wave, Model E, θ = 63 deg.

## VITA

Flight Lieutenant Sajid Hussain was born on 19 January 1951 at Rawalpindi, Pakistan. After doing F.Sc. (Pre-engineering) from Gordon College Rawalpindi in 1968, he joined the Pakistan Air Force College of Aeronautical Engineering (P.A.F. C.A.E.) from where he obtained a Bachelor Degree in Aeronautical Engineering with Honours in 1972. He served as a maintenance officer from 1973 to 1975 in one of the supersonic fighter squadrons of the Pakistan Air Force. In September 1975, he was assigned to the P.A.F. College of Aeronautical Engineering as assistant professor. In June 1976, he entered the Graduate Aeronautical Engineering program of the United States Air Force Institute of Technology to obtain an M.S. degree in Aeronautical Engineering.

Permanent address: 68-A Shafique Housing
Scheme, Rawalpindi, Pakistan

This thesis was typed by Mrs. Frances Jarnagin.

UNCLASSIFIED

SECURITY CLASSIFICATION OF THIS PAGE (When Data Entered)

| REPORT DOCUMENTATION PAGE | | READ INSTRUCTIONS BEFORE COMPLETING FORM |
|---|---|---|
| 1. REPORT NUMBER<br>GAE/AE/77D-5 ✓ | 2. GOVT ACCESSION NO. | 3. RECIPIENT'S CATALOG NUMBER |
| 4. TITLE (and Subtitle)<br>OPTICAL INVESTIGATION OF FLOW FIELD GENERATED BY NORMAL SHOCK PROPAGATION INTO A RECTANGULAR DUCT WITH IRREGULAR WALLS | | 5. TYPE OF REPORT & PERIOD COVERED<br>MS Thesis<br>6. PERFORMING ORG. REPORT NUMBER |
| 7. AUTHOR(s)<br>Sajid Hussain<br>Flight Lieutenant, P.A.F. | | 8. CONTRACT OR GRANT NUMBER(s) |
| 9. PERFORMING ORGANIZATION NAME AND ADDRESS<br>Air Force Institute of Technology (AFIT-EN) ✓<br>Wright-Patterson AFB, Ohio 45433 | | 10. PROGRAM ELEMENT, PROJECT, TASK AREA & WORK UNIT NUMBERS |
| 11. CONTROLLING OFFICE NAME AND ADDRESS | | 12. REPORT DATE<br>December 1977<br>13. NUMBER OF PAGES |
| 14. MONITORING AGENCY NAME & ADDRESS(if different from Controlling Office) | | 15. SECURITY CLASS. (of this report)<br>Unclassified<br>15a. DECLASSIFICATION/DOWNGRADING SCHEDULE |

16. DISTRIBUTION STATEMENT (of this Report)

Approved for public release; distribution unlimited

17. DISTRIBUTION STATEMENT (of the abstract entered in Block 20, if different from Report)

18. SUPPLEMENTARY NOTES

APPROVED FOR PUBLIC RELEASE AFR 190-17.

JERRAL F. GUESS, CAPT, USAF
Director of Information

19. KEY WORDS (Continue on reverse side if necessary and identify by block number)

Schlieren Optical System
Irregular Duct
Shock Wave Attenuation

20. ABSTRACT (Continue on reverse side if necessary and identify by block number)

An optical study of flow field behind a normal shock wave propagating into a rectangular duct with irregular walls was conducted in the AFIT 8 in x 4 in x 20 ft air-air shock tube. Attenuation behavior of the normal shock was also studied. An average upstream Mach number of 1.59 was maintained for all runs. A total of five wall shapes designated as A, B, C, D and E were fabricated and analyzed. Model A, a straight section, served as reference for comparative study of other models. Models B, C and D had identical wave lengths, amplitudes and maximum and minimum flow areas but their ramp angle θ was 30 deg, 60 deg and

DD FORM 1 JAN 73 1473 EDITION OF 1 NOV 65 IS OBSOLETE

UNCLASSIFIED

SECURITY CLASSIFICATION OF THIS PAGE (When Data Entered)

Continuation of Block 20. ABSTRACT

90
90 deg, respectively. Model E had a saw tooth design and all the other geometrical parameters except the wavelength and the ramp angle were similar to Models B thru D. The wavelength for Model E was half the value of other models and its ramp angle was 63 deg.

Disturbance attenuation was determined by measuring its speed across consecutive pairs of pressure transducers located at known distances along the entire length of the test section. Time interval counters measured the time lapse between transducers. Comparative study of all models revealed that disturbance attenuation depends upon the shape of the irregular wall and the two most significant factors in this regard are the ramp angle and the wave length. A higher ramp angle leads to more abrupt area reduction and provides greater attenuation. Shorter wave length provides more irregularities per unit length, which results in considerable improvement in attenuation phenomenon. Model D, $\theta$ = 90 deg is branded as the most effective design in the present study. Schlieren photographs of flow field in the irregular wall section for all models were obtained and the selected photographs are included in the report.